VI.7. COMPOSITIONAL CHANGES AND CHARACTERIZATION OF PRECIPITATED FISCHER-TROPSCH CATALYSTS IN THE SLURRY PHASE SYNTHESIS (Robert J. O'Brien, Diane R. Milburn Liguang Xu, Robert L. Spicer and Burtron H. Davis, Yong-Xi Li, K. R. P. M. Rao, Frank E. Huggins, Vikram Mahajan).

VI.7.1. INTRODUCTION

The slurry phase Fischer-Tropsch Synthesis (FTS) utilizing iron catalysts is presently considered a viable process for obtaining high quality transportation fuels, heavy waxes and chemical feedstocks from coal derived synthesis gas (VI.7.1). Slurry phase reactors have the advantage over conventional fixed-bed reactors of being able to remove the large heat of reaction of the FTS and they are less expensive to operate (VI.7.2,VI.7.3). Iron based FTS catalysts are preferred because they catalyze the water-gas shift reaction; therefore, hydrogen lean synthesis gas produced by modern coal gasifiers can be utilized (VI.7.1-VI.7.4). Iron catalysts are also much less expensive than cobalt or ruthenium FTS catalysts and are more versatile; iron catalysts can produce a product ranging from light alkenes to heavy waxes depending on the process conditions and catalyst composition (VI.7.1,VI.7.5). It is generally necessary to promote iron based catalysts with an alkali, such as potassium, to increase the production of alkenes and high molecular weight hydrocarbons and copper to facilitate iron reduction (VI.7.6,VI.7.7). Structural promoters such as silicon or aluminum are usually added to stabilize the surface area and extend the lifetime of catalysts (VI.7.8).

Substantial work has been published by several research groups utilizing fused magnetite and variously promoted precipitated iron catalysts in the slurry phase (VI.7.3). Most of these works have focused on the activity and product selectivity of these catalysts with little attention on catalyst characterization. Considerable efforts have been made to determine the bulk composition of iron catalysts during the FTS; however, many of these have utilized in situ Mössbauer spectroscopy (VI.7.9-VI.7.12) or XRD (VI.7.13,VI.7.14) under low CO and H_2 conversions at low pressure. At low synthesis gas conversions the reactor atmosphere is reducing and the bulk composition of iron catalysts is usually a mixture of χ-Fe_5C_2 and ϵ'-$Fe_{2.2}C$. Bulk phase characterization of iron catalysts under industrial conditions, ie. high conversion and medium pressure, have usually been carried out in fixed bed and slurry reactors (VI.7.5,VI.7.6,VI.7.16-VI.7.22). Characterization of catalysts used in fixed bed reactors is not straight forward because the entire catalyst bed does not see the same conditions. The conditions are reducing in the reactor where the synthesis gas is introduced and tend to be oxidizing at the exit end of the reactor because of a high level of CO_2 and H_2O; this will result in the catalyst existing as iron carbides at the top of the reactor and predominantly iron oxide(s) at the bottom of the reactor. One way around this problem is to study the catalysts in a slurry reactor. All of the catalyst sees essentially the same conditions in a slurry reactor because the catalyst-oil slurry is well mixed. Using a slurry phase reactor makes it more facile to determine the effects of promoters on the catalyst structure and composition during the FTS.

The present study focuses on the effect of potassium, copper, silicon and aluminum on the FTS activity and composition and of iron based, precipitated

catalysts. Catalysts were run in the slurry phase in a continuous stirred tank reactor under industrial conditions. Catalyst samples were periodically withdrawn from the reactor and studied by XRD, Mössbauer spectroscopy, BET analysis and elemental analysis.

VI.7.2. EXPERIMENTAL

Catalysts were prepared by continuous precipitation of ferric oxyhydroxide from 1.17 M $Fe(NO_3)_3 \bullet 9H_2O$ and concentrated NH_4OH solutions at pH of ~9.5. Catalysts containing Si or Al were prepared by adding hydrolyzed $Si(OC_2H_5)_4$ or $Al(NO_3)_3 \bullet 9H_2O$ to the $Fe(NO_3)_3 \bullet 9H_2O$ solution. All catalysts were oven dried under a stream of air at 110°C until no weight loss occurred. Promotion with potassium was accomplished by adding the appropriate amount of potassium t-butoxide to the catalyst oil slurry in the Fischer-Tropsch reactor. Copper promotion was carried out analogously with basic cupric carbonate. The nominal catalyst compositions given as atomic % relative to iron metal with their corresponding run numbers are shown in Table VI.7.1.

Catalysts were tested in either a one L or 300 cc autoclave operated as a continuous stirred tank reactor. The catalysts were suspended in a hydrocarbon oil supplied by Ethyl which has a carbon number range of about C_{25}-C_{30}. In all cases the catalyst loadings were 20 wt %. A schematic of the on L reactor system is shown in Figure VI.7.1. The H_2 and CO feed gas flow rates were controlled by two mass flow controllers supplied by Brooks instruments. The H_2/CO feed ratios wee consequently controlled by changing the flow rates of the appropriate gas. The resulting synthesis gas was delivered to the catalyst slurry through a 1/8" i.d. dip tube that ran to the bottom of the reactor below the impeller blade. The reactor was equipped with three

traps maintained at nominal temperatures of 200°C, 60°C and 0°C. The 200°C trap was connected to a line fitted with a 0.5 μm filter. The filter was placed approximately 2" inside the reactor from the top. This permitted for removal of accumulated wax inside the reactor. The reactor traps could be operated in two ways. The reactor effluent could be sent through the filter which would then go to the 200°C trap followed by the 60°C and 0°C traps or the filter could be bypassed and the effluent sent to the 60°C trap. Generally the reactor was operated bypassing the filter. This was done to prevent excessive loss of the start-up oil. To prevent the reactor from filling with high molecular weight products, the 200°C trap was operated for 2 hr every 24 hr. This proved sufficient to keep the slurry level at about 500 cc. Uncondensed effluent was vented to atmospheric pressure and was directed to on-line gas analyzers. A Carl gas analyzer was used to analyze for C_1-C_4 hydrocarbons, CO, H_2, and CO_2; a Hewlett-Packard 5790 GC equipped with a porpack-Q column was used for analysis of C_4-C_9 hydrocarbons. The oil and wax products collected in the 60°C and 0°C traps were analyzed with a Hewlett-Packard 5890 GC equipped with a DB-5 capillary column. Aqueous phases were analyzed with a Hewlett-Packard 5790 GC equipped with a porpack-Q column.

The reactor was also fitted with a 1/8" dip tube equipped with a high temperature valve which enabled catalyst slurry samples to be removed periodically during the pretreatment and synthesis for characterization studies.

All of the catalysts used in this study were pretreated with CO at 175 psig. The CO feed was started at 2.0 nL/hr-g(Fe) and the temperature of the reactor ramped from 25°C to 270°C at 2.0°C/min. The reactor temperature was maintained at 270°C for 24 hr. Following the pretreatment, hydrogen was started giving a synthesis gas

with $H_2/CO=0.7$ at 3.4 nL/hr-g(Fe) at 175 psig. Synthesis gas conversions were determined by measuring the exit stream flow rate with a bubble film flow meter and by gas chromatography of the exit stream.

VI.7.2.a. Catalyst Characterization

Mössbauer Spectroscopy. Mössbauer spectra of the catalyst samples were obtained from a constant acceleration spectrometer. The γ-ray source consisted of 50-100 mCi of ^{57}Co in a Pd matrix. Spectra were analyzed using a least-squares fitting routine with the iron content of each phase determined from their relative peak areas.

X-ray Diffraction. Powder X-ray diffraction patterns of the catalysts were obtained using a Philips APD X-ray diffraction spectrometer equipped with a Cu anode and Ni filter operated at 40 Kv and 20 Ma ($CuK\alpha=1.5418$ Å). Iron phases were identified by comparing diffraction patterns of the catalyst samples with those in the standard powder X-ray diffraction file compiled by the Joint Committee on Powder Diffraction Standards published by the International Center for Diffraction Data.

BET Surface Area Determination. Nitrogen adsorption measurements were made with a Quantachrome Autosorb 6 instrument. Samples were outgassed at 80°C and less than 50 mtorr for a minimum of 12 hr prior to analysis. BET surface areas and pore size distributions were calculated from the adsorption and desorption data, respectively.

VI.7.2.b. Catalyst Testing

RJO-168. The Fischer-Tropsch activity for iron catalysts can be approximated by the conversion level of CO and H_2. The unpromoted catalyst started with a CO and H_2 conversion of about 72% and rose to 84% and 77% respectively (Figure

VI.7.2). The conversion declined steadily over the coarse of the run and at approximately 150 hr of synthesis the H_2 conversion became higher than the CO conversion. This occurred at a conversion of about 70%. After 340 hr of synthesis, the CO conversion had declined to 26% and the H_2 conversion was 45%.

The water-gas shift (WGS) activity of the catalyst can be followed by monitoring the fraction of carbon converted to CO_2, assuming CO_2 is produced only by the WGS. The overall reaction scheme for the iron catalyzed FTS can be expressed as

$$CO + 2H_2 \rightarrow -CH_2- + H_2O$$

$$H_2O + CO \rightarrow CO_2 + H_2$$

$$2CO + H_2 \rightarrow -CH_2- + CO_2$$

When the WGS is complete, the ratio of CO_2 formed to CO converted is 0.5. For the unpromoted catalyst, this ratio was constant at 0.45 for the first 160 hr of synthesis and then decreased to 0.33 after 340 hr. A better measure of the extent of the WGS is to determine the reaction quotient, $K_{app}=[CO_2][H_2]/([CO][H_2O])$. The equilibrium value of the reactor quotient at 270°C is approximately 65. A plot of K_{app} vs. time of synthesis, Figure VI.7.3, shows that the WGS activity decreases with the CO conversion, declining from about 9.6 to 1.2 at 216 hr of synthesis. In short the unpromoted catalyst had poor WGS activity.

Alkane/alkene product selectivity for the C_2, C_3 and C_4 fractions are shown in Figure VI.7.4. In general, the alkane fraction was higher for C_2 (86-65%) than C_3 (39-19%) or C_4 (26-17%). At high conversions the alkane selectivity was highest but it appeared to level off below 50% CO conversion.

A measure of the secondary reactions of a FTS catalyst can be made by monitoring the fraction of internal alkenes to 1-alkenes. It is believed that only 10% of the alkenes synthesized as primary products are internal alkenes; however, internal alkenes can also be synthesized by readsorption followed by isomerization of 1-alkenes:

$$R\text{-}CH_2\text{-}CH{=}CH_2 \leftrightarrow R\text{-}CH{=}CHCH_3 \quad \text{(VI.7.23)}.$$

A plot of the 1-alkene to total alkene ratio for the C_4 fraction as a function of time is shown in Figure VI.7.4. At the beginning of the synthesis, 2 hr, the ratio was 0.67; however, it rapidly decreased to 0.44 after 24 hr of synthesis. During the remainder of the run the 1-alkene fraction increased to 0.67 as the CO conversion decreased. This seems to indicate, as expected for an unpromoted catalyst, that secondary reactions were significant.

Methane and ethane selectivities are shown in Figure VI.7.5. The methane selectivity decreased from 9% to 5% as the CO conversion decreased from 84 to 77%; however, it steadily increased thereafter despite the continuous decrease in activity. The methane+ethane selectivity followed a similar trend.

Total hydrocarbon production paralleled the conversion data (Figure VI.7.5), increasing to 166 g/m^3 synthesis gas after 48 hr and decreasing steadily to 63 g/m^3 at the end of the run. The C_3+ hydrocarbon production followed a similar trend, reaching a maximum of 145 g/m^3 at 48 hr and decreasing to 53 g/m^3 at 336 hr. The maximum values fall short of the target goal of 178 g/m^3 total hydrocarbon and 88% C_3+ selectivity.

RJO-169. Promotion of the catalyst discussed above with 0.71 at.% potassium had little effect on the activity of the catalyst (Figure VI.7.6). The CO and H_2 conversions were 66% and 58% after 3.5 hr of synthesis and rose to a maximum of 82% and 67%, respectively after 24 hr. The conversions decreased during the remainder of the run at a higher rate than the unpromoted catalyst.

The CO_2/CO ratio for this run remained constant at about 0.48 indicating substantial WGS activity (Figure VI.7.7). This is confirmed by the WGS reaction coefficient, K_{app}, which was 24 after 24 hr or 35% of the equilibrium value. The WGS activity decreased steadily as the CO conversion decreased and reached 8.8 after 145 hr at 46% CO conversion.

The alkene production was excellent for the C_2, C_3 and C_4 hydrocarbon fractions. The C_2 alkene fraction oscillated between 0.19 and 0.36 while the C_3 and C_4 fractions remained fairly constant at about 0.17 and 0.13, respectively (Figure VI.7.8). Based on this data very little secondary reactions, ie. alkene hydrogenation, occurred for the C_3 and C_4 fractions. This is substantiated by the 1-alkene fraction of the C_4 product remaining at about 95% throughout the run (Figure VI.7.8).

Methane and ethane selectivity were also good for this run. Methane production remained below 5% for the duration of the run while the methane and ethane combined production was below 6% due to the excellent ethylene selectivity of the catalyst (Figure VI.7.9). Hydrocarbon production was poor even at the beginning of the run when conversion was high. The total hydrocarbon production was below 160 g/m^3 synthesis gas during the first 24 hr of the run and declined to 87g/m^3 after

145 hr. The C_3+ production followed the same trend reaching a maximum of 142 g/m^3 and declining to 79 g/m^3 (Figure VI.7.9).

RJO-137. The initial activity of the 4.4 at.% silicon, 0.71 at.% potassium promoted catalyst was similar to that of the above mentioned catalyst, starting at 71% CO and 67% H_2 conversion after 3 hr. During the next 72 hr, the CO conversion reached a maximum of 93% and essentially declined at a rate of 0.5% per day up to 263 hr where it reached 84%; thereafter, it remained constant for the remainder of the run. The H_2 conversion followed a similar trend declining from a maximum of 82% to 71% (Figure VI.7.10). The CO conversion reached our target of 90%; however, the H_2 conversion was below our goal of 88%. This was probably due to a fairly large amount of H_2 being produced by the WGS reaction. The CO_2/CO ratio was as high as 0.50 and averaged about 0.48-0.49 throughout the run (Figure VI.7.11). The reaction coefficient for the WGS was as high as 36, 58% of the equilibrium value. The WGS activity declined steadily as the run progressed, reaching K_{app}=22 after 454 hr (Figure VI.7.11).

The C_2, C_3 and C_4 alkane/alkene selectivity is shown in Figure VI.7.12. During the steady state of the run, the C_2 alkane fraction was about 0.9; much higher than the unpromoted or 0.5% potassium promoted catalysts. The C_3 and C_4 alkane fractions were 0.42 and 0.3 respectively. The 1-alkene fraction of the total C_4 alkene was about 0.38 during the steady state period; however, it was higher earlier in the run and declined rapidly over the first 72 hr of the run (Figure VI.7.12). This indicates that this catalyst promoted a large amount of secondary reactions. Methane and ethane selectivity was poor for this catalyst starting at 7% for methane and 12% for methane

and ethane combined. Both of these products selectivities increased during the run, despite a slight decrease in conversion (Figure VI.7.13).

Total and C_3+ hydrocarbon production appeared to oscillate during the run. The maximum total production was about 175 g/m^3 synthesis gas (Figure VI.7.13). The corresponding C_3+ production was 149 g/m^3. The total hydrocarbon production met our target goal of 173g/m^3; however, the C_3+ production was slightly lower than the target value of 156g/m^3.

RJO-163. This run used a the same catalyst composition as *RJO-137*; however, 2.6 at.% Cu (based on Fe) was added to the catalyst. Similar results were obtained for this run. The major difference is the conversion was about 4% lower and the catalyst was not as stable during the first 360 hr of synthesis. After one hr of synthesis the CO conversion was 54%, after 4 hr it had risen to 75%. The CO and H_2 conversions continued to rise to maxima of 90 and 81%, respectively after 50 hr of synthesis (Figure VI.7.14). The catalyst deactivated somewhat the next 240 hr, decreasing to 74% CO and 68% H_2 conversion. Approximately the same WGS activity was found for this catalyst with a CO_2/CO ratio slightly exceeding 0.5 at times and a WGS reaction coefficient between 20 and 30 during most of the run (Figure VI.7.15).

The C_2, C_3 and C_4 alkene/alkane selectivities are shown in Figure VI.7.16. The C_2 fraction was approximately 90% alkane as was the case for *RJO-137*; however, the C_3 and C_4 products were slightly more paraffinic with selectivities of about 0.5 and 0.33, respectively. The 1-alkene selectivity for the C_4 alkene fraction was correspondingly low at about 35% (Figure VI.7.16).

The methane and ethane selectivities mirrored that of *RJO-137* (Figure VI.7.17). The methane selectivity started at 8.8%, decreased to 6.5% after 80 hr and steadily increased to 10% after 290 hr. Similarly methane and ethane combined selectivity declined from an initial value of 13% to 11.5% after 80 hr and then rose to 18% at the end of the run. The maximum hydrocarbon production of 176 g/m^3 met our target value as did the maximum C_3+ production of 153 g/m^3 (Figure VI.7.17). However, the hydrocarbon productions declined rapidly to 134 g/m^3 after 290 hr of synthesis.

RJO-164, RJO-165 and RJO-166. Three runs were made using a ferric oxyhydroxide catalyst promoted with 4.4 at.% Al. These runs were made with 0.71, 2.8 and 7.0% at.% potassium promotion in an attempt to see what affect moderate to high potassium loadings have on iron catalysts. Since these runs were conducted in 300 cc reactors, only about 16 g of catalyst was loaded which limited the number of catalyst samples which could be taken. This meant that the runs only lasted 72 hr because of depletion of the catalyst.

In general, the catalyst activity decreased with increasing potassium content. The 0.71 at.% potassium catalyst followed a similar activity trend as mentioned previously; the CO and H_2 conversions rose from initial values of 61% and 56%, respectively to 84% and 72% after 24 hr. These remained steady for the remainder of the run (Figure VI.7.18). The run with 2.8 at.% potassium loading started with CO and H_2 conversions of 42% and 30%, respectively. They rose to 69% and 55% after 24 hr but declined to 31% and 28% after 72 hr (Figure VI.7.19). The catalyst with 7.0 at.% potassium started with lower CO and H_2 conversions of 30 and 22% and peaked at 54% and 47% (Figure VI.7.20). This catalyst showed more stability than the 2.8 at.%

potassium catalyst. This may be within experimental error, since the runs were only 72 hr long, the catalysts had not reached steady state, ie. the 7.0 at.% potassium catalyst may have declined in activity if allowed to run longer.

Since liquid products were not collected for these runs, the reaction coefficient for the WGS could not be determined. For the 0.71 at.% potassium catalyst, the CO_2/CO ratio of ~0.5 indicates a fairly high WGS activity. The 2.8 at.% potassium catalyst had CO_2/CO substantially above 0.5 (~0.58), indicating the deposition of carbon via the Boudouard reaction:

$$2CO \rightarrow C + CO_2.$$

The catalyst with 7.0 at.% potassium had a CO_2/CO ratio of ~0.4 (Figure VI.7.21).

The alkane/alkene selectivities are shown in Figures 22 to 24. Surprisingly, the C_3 and C_4 alkene selectivities are approximately equivalent for these catalysts ranging from 80-85%. However, the C_2 selectivity was 25% alkene for the 0.71 at.% potassium catalyst as compared to 75-70% for the 2.8 at.% and 7.0 at.% potassium catalyst.

The 1-alkene fraction of the total C_4 alkene was about 72% after declining from an initial value of 92% for the 0.71 at.% potassium catalyst. The 2.8 at.% and 7.0 at.% potassium catalysts had values of about 95% 1-alkene (Figure VI.7.25). These results are much in line with the high alkene selectivity of the catalysts, indicating low secondary reactions.

Methane selectivity decreased with increasing potassium content; however, this also may be influenced by differences in the activities of the catalysts and not necessarily the differences in potassium content. The 0.71 at.% potassium catalyst had an initial methane selectivity of 5% which rose steadily to 7%. Methane selectivity

for the 2.8 at.% and 7.0 at.% potassium catalysts were 5% and 4%, respectively (Figure VI.7.26).

VI.7.2.c. Catalyst Characterization

XRD and Mössbauer Spectroscopy. In general, all of the catalysts were found by XRD to be rapidly and completely reduced to Fe_3O_4 during the first 2 hours of CO pretreatment. Further reduction to iron carbides proceeded much more slowly and showed a dependence on the promoters used. It is believed that iron oxide catalysts are reduced by CO to Fe_3O_4 in a two step process:

$$3Fe_2O_3 + CO \rightarrow 2Fe_3O_4 + CO_2$$

$$5Fe_3O_4 + 32CO \rightarrow 3Fe_5C_2 + 26CO_2,$$

where Fe_5C_2 is the approximate stoichiometry of the resulting iron carbide (VI.7.13,VI.7.17,VI.7.18). Berry and Smith found that the first step of the reduction occurs at the same rate for unpromoted and potassium promoted catalysts; however, they found the second step occurred faster for a potassium promoted catalyst (VI.7.13). It was concluded that potassium accelerates the rate of dissociative chemisorption of CO on Fe_3O_4 by increasing the amount of back-donation of electrons to the CO molecule.

Following reduction to Fe_3O_4, the unpromoted catalyst, *RJO-168* , was slowly reduced to a mixture of χ-Fe_5C_2 and ϵ'-$Fe_{2.2}C$. The catalyst was not completely converted to iron carbides during the pretreatment; in fact, the 311 line of Fe_3O_4 was the most intense peak in the XRD diffractogram. Iron carbides synthesized during the FTS tend to be somewhat amorphous and give weak XRD peaks, so although the iron carbide peaks are weaker than the Fe_3O_4 peaks, iron carbide may be the dominant

phase. In fact, the catalyst was probably converted to mostly iron carbides, since the Fe_3O_4 peaks were about 25% as intense as they were following 2 hr of exposure to CO. XRD of the pretreated catalyst following exposure to synthesis gas clearly shows that the iron carbides are partially reoxidized to Fe_3O_4 (Figure VI.7.27). This presumably is due to the oxidizing nature of H_2O and CO_2 which are formed as by-products of the FTS. Peaks corresponding to χ-Fe_5C_2 and ϵ'-$Fe_{2.2}C$ were present throughout the synthesis; however, it is difficult to determine which was the most abundant.

XRD results of the 0.71 at.% potassium promoted catalyst, *RJO-169*, are very similar to the unpromoted catalyst during the pretreatment. The catalyst was rapidly converted to Fe_3O_4 during the period in which the catalyst was heated from room temperature to 270°C under CO. Subsequent reduction to iron carbides was incomplete following an additional 24 hr or pretreatment. χ-Fe_5C_2 and ϵ'-$Fe_{2.2}C$ carbides were both present although the ratio of Fe_3O_4 to iron carbide peak intensities appeared to be higher for this run than for the unpromoted catalyst. This may indicate that the catalyst did not carbide to the same extent as the unpromoted catalyst which contradicts the results of Berry and Smith (VI.7.13).

XRD revealed that subsequent exposure to synthesis conditions brought about an increase in the carbide content of the catalyst. Following 150 hr of synthesis the catalysts had been almost completely converted to ϵ'-$Fe_{2.2}C$; with small amounts of χ-Fe_5C_2 and Fe_3O_4 also present (Figure VI.7.28). It is surprising that this catalyst carbided during the synthesis because the total synthesis gas conversion was as high as 76%; this is high enough to produce an oxidizing environment in the reactor from

H_2O and CO_2. It is possible that accumulated carbon on the catalyst prevented the carbide from being reoxidized.

The silicon and potassium promoted catalyst, run *RJO-137*, behaved very similarly to the unpromoted catalyst. XRD showed a large amount of χ-Fe_5C_2 and ϵ'-$Fe_{2.2}C$ were formed during the pretreatment; although, Fe_3O_4 was also present. During the first 4.5 hr of synthesis the carbide peaks grew slightly; however, additional exposure to synthesis gas caused the carbides to gradually oxidize to Fe_3O_4; after 320 hr of synthesis the catalyst appeared to be pure Fe_3O_4. During the final 140 hr of synthesis, the carbide content increased slightly.

Mössbauer spectroscopy results for *RJO-137* are shown in Figures 29 and 30. It was found that after 7.75 hr of CO pretreatment at 270°C and 175 psig the catalyst was essentially 34% magnetically ordered Fe_3O_4 with the remainder a superparamagnetic species. The quadrupole moment, 0.80, and isomer shift, 0.47, are consistent with small iron oxide. Following 24 hr at pretreatment conditions, the catalyst was 37% magnetically ordered Fe_3O_4 with the remainder 24% χ-Fe_5C_2 and 39% superparamagnetic. The superparamagnetic doublet at the end of pretreatment was substantially different than after 7.75 hr of pretreatment indicating a phase transition. At the end of the pretreatment the quadrupole moment had increased to 1.21 mm/s. This indicates the presence of small particle iron carbide. Amelse et al. have reported similar results and have assigned the superparamagnetic doublet to ϵ'-$Fe_{2.2}C$ (VI.7.12). During the first 28 hr of synthesis the χ-Fe_5C_2 and superparamagnetic carbide components increased to 34% and 50%, respectively. During the next 292 hr of synthesis the χ-Fe_5C_2 and the superparamagnetic

components decreased dramatically to 0% and 17%, respectively, while the Fe_3O_4 content increased to 83%.

Copper has been implicated in aiding the reduction of iron catalysts with H_2 by lowering the reduction temperature, thereby decreasing the amount of sintering of the catalysts (VI.7.6,VI.7.7). The silicon and potassium promoted catalyst was treated with 2.6 at.% Cu, *RJO-163*, in an attempt to determine the affect of copper on catalysts pretreated with CO. XRD results show essentially no difference between the silicon and potassium promoted catalyst with (*RJO-163*) and without (*RJO-137*) copper (Figure VI.7.31). No change in the type of carbide formed or the extent of carbiding could be detected by XRD of the pretreated catalyst; however, the copper promoted catalyst appeared to contain more iron carbides during the synthesis. SEM of the copper promoted catalyst indicates that the copper sintered during the pretreatment. It is plausible that a lack of an even distribution of copper across the catalyst surface inhibited the promoting effects of the copper. An industrially prepared catalyst containing potassium, kaolin and copper, which shows a better distribution of copper, was reduced completely to a mixture of χ-Fe_5C_2 and ϵ'-$Fe_{2.2}C$ during the same pretreatment procedure used for *RJO-163*, so the results of the present study are not conclusive.

Mössbauer and XRD results of the CO pretreated, 4.4 atomic% aluminum catalyst promoted with 0.71, 2.8 and 7.0 at.% potassium: *RJO-164*, *RJO-165* and *RJO-166*, respectively, did not show any correlation between carbide content and potassium concentration. XRD indicated a large amount of χ-Fe_5C_2 and ϵ'-$Fe_{2.2}C$ were formed during the pretreatment of the 0.71% potassium promoted catalyst.

Mössbauer spectroscopy showed 70% χ-Fe_5C_2 and 10% superparamagnetic carbide, consistent with small particle ϵ'-$Fe_{2.2}C$. The XRD results of this catalyst during the ensuing synthesis were similar to the unpromoted catalyst (*RJO-168*) and the silicon/potassium promoted catalyst (*RJO-137*). Mössbauer spectroscopy revealed that during synthesis the χ-Fe_5C_2 carbide was oxidized to Fe_3O_4 while the superparamagnetic component increased slightly; following 72 hr of synthesis, 84% of the iron was present as Fe_3O_4 while 16% was present as superparamagnetic carbide. The aluminum catalyst with 0.71 at.% potassium reoxidized at a higher rate than the silicon promoted catalyst with the same potassium level in which it took over 300 hr to produce as much Fe_3O_4.

Increasing the potassium level to 2.8 at.% decreased the amount of carbide that formed during the pretreatment to 38% (34% χ-Fe_5C_2 and 4% superparamagnetic). During the synthesis, the iron content present as iron carbide increased to 41% ϵ'-$Fe_{2.2}C$, 6% χ-Fe_5C_2 and 10% superparamagnetic carbide. The catalyst promoted with 5.0% potassium carbided to 34% χ-Fe_5C_2, 23% ϵ'-$Fe_{2.2}C$ and 9% superparamagnetic. Following 72 hr of FTS, the catalyst was reduced further to 34% ϵ'-$Fe_{2.2}C$, 20% χ-Fe_5C_2 and 21% superparamagnetic carbide. The increased carbide content for the 2.8 at.% and 7.0 at.% potassium promoted catalysts may be due to lower activities of these catalysts compared to *RJO-164*. The lower activity would provide a more reducing atmosphere in the reactor. It is interesting that the high loadings of potassium for *RJO-165* and *RJO-166* seemed to promote the formation of magnetically ordered ϵ'-$Fe_{2.2}C$ (Figure VI.7.32).

BET Surface Area, Pore Volume and Pore Size Distributions. BET data are listed in Tables VI.7.2-VI.7.8. The surface area and pore volume of the as prepared catalysts are as follow: unpromoted catalyst-124 m^2/g, 0.088 cm^3/g; 4.4% Si catalyst- 284 m^2/g, 0.226 cm^3/g; 4.4 Al catalyst- 160 m^2/g, 0.130 cm^3/g. Surface area as a function of time on stream for the catalysts used in this study are shown in Figures 33 and 34. In general, all of the catalysts rapidly decrease in surface area during the initial 3-8 hours of the CO pretreatment. This can be explained as a breakdown of the pore structure of the ferric oxy/hydroxide catalyst upon conversion to Fe_3O_4 and, ultimately, to χ-Fe_5C_2 and ϵ'-$Fe_{2.2}C$. Except for RJO-165 and RJO-166 where high levels of potassium were used, the surface areas and pore volumes of the catalysts tend to increase during the synthesis stage of the runs. The pore size distributions of the catalysts tend to broaden with time on stream and the distribution has a tendency to shift to wider pores, particularly with runs *RJO-137*, *RJO-163* and *RJO-164* (Figure VI.7.35).

Silicon and aluminum appeared to help stabilize the surface area of the catalysts as compared to the unpromoted and potassium promoted catalysts. Surface areas for the silicon and aluminum promoted catalysts with 0.71 at.% potassium were about 65-70 m^2/g following CO pretreatment as compared to 20 m^2/g for the catalysts with no silicon or aluminum. In addition the aluminum and silicon promoted catalysts had smaller pores and narrower pore size distributions than the catalysts with no structural promoters (Figure VI.7.36). Comparing *RJO-168* and *RJO-169* shows that the promotion of the ferric oxyhydroxide catalyst with 0.71 at.% potassium had no effect on the surface area of the catalyst during the CO

pretreatment; however, the surface area of the potassium promoted catalyst increased more quickly than the unpromoted catalyst during the synthesis. This may be due to a higher rate of deposition of porous carbon on the potassium promoted catalyst.

The effect of increasing potassium loading on the aluminum promoted catalyst is seen in Figure VI.7.34. The catalyst with 0.71 at.% potassium had a surface area following pretreatment of 70 m^2/g as compared to 58 m^2/g and <3 m^2/g for the 2.8 and 7.0 at.% potassium promoted catalysts. No trend could be seen between the potassium loading and the pore size distributions and pore size for this series of catalysts. This is probably because the catalyst promoted with 5.0% potassium had a type II isotherm characteristic of a nonporous material.

VI.7.3. DISCUSSION

Promotion of iron oxide with 0.71 at.% potassium (*RJO-169*) had essentially had no effect on the activity of the catalyst; however, it increased the rate of catalyst deactivation. The rapid deactivation of the potassium promoted catalyst may be due to an increase in the deposition of carbonaceous material which cover active sites (Figure VI.7.37). On the other hand, promotion of the 0.71 at.% potassium/iron oxyhydroxide catalyst with silicon (*RJO-137*) increased the activity as well as the stability of the catalyst. This presumably is related to silicon increasing and stabilizing the effective surface area of the catalyst. Likewise, promotion of 0.71 at.% potassium/ferric oxyhydroxide with aluminum (*RJO-164*) helped stabilize the CO conversion during the first 72 hours of synthesis; however, it did not increase the initial activity above that of the unpromoted (*RJO-168*) or the 0.71 at.% potassium (*RJO-169*)catalysts despite having a surface area comparable to the same catalyst with

silicon. Increasing the potassium level but keeping the aluminum level constant was found to decrease the surface area and the initial activity of the catalysts; no trend in stability could be discerned because of the shortness of the runs.

Promoter effects on product selectivity are shown in Table VI.7.9. Data were taken at 82-85% CO conversion. It is best to compare product selectivity data of different catalysts at comparable activity because selectivities will change with changes in conversion. For example, with increasing CO conversion, methane selectivity will increase and alkene selectivity will tend to decrease. It is clear from Table VI.7.9 that promotion of unsupported iron oxyhydroxide with 0.71 at.% potassium increases the C_2-C_4 alkene selectivity and the 1-alkene selectivity of the C_4 alkene. This is indirect evidence that potassium promotion inhibits secondary reactions such as alkene hydrogenation and isomerism. In addition, 0.71 at.% potassium promotion lowers the methane selectivity from 7.0% to 4.0% and substantially increases the WGS activity. The total hydrocarbon production for the 0.71 at.% potassium promoted catalyst decreased substantially from 165 g/m^3 of synthesis gas to 155 g/m^3. This decrease is undoubtedly due to an increase in the WGS activity of the potassium promoted catalyst; more CO was converted to CO_2 and less to hydrocarbons. It is; however, apparent that potassium increased the selectivity of C_3+ products from 85% to 91%. Much of this can be explained by CO and H_2 chemisorption studies on iron catalysts. Dry determined that potassium promotes the dissociative chemisorption of CO on iron catalysts and decreases the chemisorption of hydrogen (VI.7.24). This essentially means that potassium increases the C:H ratio on the surface of iron catalysts. This in turn increases the probability of chain growth and decreases the odds of termination

as an alkane and the secondary hydrogenation of alkene products. It is interesting that the silicon and aluminum promoted catalysts with 0.71 at.% potassium have selectivities more like those of the unpromoted catalysts than the 0.71 at.% K promoted catalyst. This may be explained by a neutralization of the basicity of the potassium by acidic silicon and aluminum. The potassium may be tied up as a silicate or aluminate; further experiments will be necessary to determine the fate of the potassium. We have identified a potassium iron hydroxysilicate with a spent industrial catalyst by XRD and Mössbauer spectroscopy; however, this catalyst contained 5 wt% K and 30 wt% SiO_2, which is much larger than that used in *RJO-137*.

Typical plots of the alkane/alkene selectivity versus carbon number are shown for *RJO-168*, *RJO-169*, *RJO-137* and *RJO-163* in Figure VI.7.38. It is difficult to make a direct comparison between the catalysts because the selectivity data were obtained at different conversions. In general, the alkene content reaches a maximum with the C_4 fraction and decreases very rapidly with increasing carbon number for the unpromoted and Si promoted catalysts and reaches 0% at $\sim C_{20}$. The potassium promoted catalyst, *RJO-169*, had essentially a constant alkene content (80%) between C_2 and C_{12}; however, the alkane fraction increased to about 75% at C_{30}. Data for *RJO-168* and *RJO-169* were obtained at '48% CO conversion and it is clear that potassium promotion increased the alkali content even at high carbon number.

A typical Anderson-Schulz-Flory plot describing the carbon number distribution of the product is shown in Figure VI.7.39 for RJO-163. The plot is a classical ASF distribution for an iron based catalyst showing two distinct slopes. Modelling the data by the method of Satterfield, gives α_1=0.65, α_2=0.86 and ζ=10.3 (VI.7.25). Similar

plots were obtained for *RJO-168* and *RJO-169* and *RJO-137* and the results are shown in Table VI.7.10. No distinct break point could be detected for *RJO-168* or *RJO-169* because the reaction had not run long enough to minimize reactor hold-up of high molecular weight products. Because of this, the effect of promoters on the product distribution are difficult to detect.

Bukur reports that copper increases secondary reaction but also increases activity of the catalyst (VI.7.7). Comparing *RJO-137* to *RJO-163* shows no beneficial promotion by 2.6 at.% copper. Alkene selectivity and 1-alkene selectivity and hydrocarbon production all three decreased. No increase in activity was observed by copper promotion and the stability of the catalyst was found to decrease substantially. Copper had essentially no effect on the surface area or pore volume of the catalyst; however the pore size distributions were substantially broader.

It is interesting that the catalysts without structural promoters, *RJO-168* and *RJO-169* both lose porosity and surface area during CO pretreatment but then regain essentially the same pore structure of the untreated catalyst following synthesis (see Tables VI.7.2-VI.7.8). Catalysts containing 4.4 at.% silicon or aluminum with the same potassium loading as *RJO-169* remain porous during pretreatment and synthesis; the only significant changes being a shift to larger pores with a wider size distribution as synthesis progresses. Based on elemental analysis, it is clear that all of the catalysts, excluding the silicon promoted, produced carbon during CO pretreatment in excess of that needed for stoichiometric iron carbide. The BET surface area and pore volume of the unsupported catalysts decrease considerably during the pretreatment as would be expected if the catalyst particles were encapsulated by nonporous carbon.

Surprisingly the surface area and the pore volume of the catalysts used in runs *RJO-137*, *RJO-163* or *RJO-164* did not decrease during the CO pretreatment. The silicon promoted catalysts, *RJO-137* and *RJO-163* had little if any carbon in excess of that present as iron carbide; however, the aluminum promoted catalyst, *RJO-164*, produced about twice as much carbon as needed to form χ-Fe_5C_2. These differences can be reconciled if different types of carbon are formed during the CO pretreatment. Sault and Datye have reported that CO pretreatment at 280°C of a doubly promoted potassium/copper catalyst results in the growth of graphitic carbon filaments and porous carbon (VI.7.26). It is possible that the catalysts lacking silicon or aluminum formed nonporous graphitic carbon preferentially while the catalysts promoted with silicon or aluminum formed predominantly porous carbon. The question of why the surface area and porosity of the unsupported catalysts recover during the FTS arises. This is probably brought about by hydrogenation of the graphitic carbon which would clean out the pores of the catalyst thus restoring the BET surface area. This could explain the high yields of methane that occur during the beginning of the reaction (Figures VI.7.5 and VI.7.9) for *RJO-168* and *RJO-169*. Deposition of porous carbon during the FTS is also apparent by comparing the BET surface area and pore volumes with the carbon content of the catalysts (VI.7.27). In general the surface areas and pore volumes increase as the carbon content increases. No correlation between carbon content and deactivation of the catalysts can be made with the current data. *RJO-168* and *RJO-169* deactivated rapidly over the first 200 hr of synthesis while *RJO-137* remained very stable during the 460 hr run. In all three cases the carbon content of the catalysts rose in excess of 20 wt.%; in fact, the carbon

content of the catalyst at the end of *RJO-137* was ~30%. TEM and high resolution SEM experiments need to be performed to determine the nature of the carbon during deactivation and when the catalyst activity is stable. It could be that at high activity porous carbon is formed while graphitic carbon is formed during deactivation.

The active phase or site of iron based FTS has been debated for years. Fischer and Tropsch proposed that iron carbides (VI.7.28) are the active phases while others have proposed that iron oxides such as Fe_3O_4 are active (VI.7.29). The current results of this study seem to imply that the bulk phases of the iron catalysts do not participate directly in the Fischer-Tropsch synthesis. This is clearly demonstrated by comparing the activity data with Mössbauer spectroscopy and XRD results for runs *RJO-137* and *RJO-164*. Both of these catalysts had stable activity after reaching their maximum conversions; *RJO-137* lost only about 3% CO conversion over a 320 hr period. Although the activities were stable for these catalysts, the catalysts bulk compositions were not. Over the course of the synthesis, *RJO-137* went from about 37% Fe_3O_4 to 83% Fe_3O_4 after 320 hr of synthesis. Correspondingly, *RJO-164* changed from 24% Fe_3O_4 to 84% Fe_3O_4 after 72 hr of synthesis. If the carbide theory were valid then the activities of these catalysts would have dropped as the carbide content decreased. Likewise, the activity would have increased as the Fe_3O_4 content increased, if Fe_3O_4 is the active phase of the FTS. Close examination of the iron composition of the different carbides shows no correlation between activity and the amount of χ-Fe_5C_2, ϵ'-$Fe_{2.2}C$ or superparamagnetic carbide. The carbide ϵ'-$Fe_{2.2}C$ is not present during the first 72 hours of synthesis and then disappears some time after 175 hours. In addition the χ-Fe_5C_2 and superparamagnetic iron carbide content reach

maxima at 72 hours and then decrease steadily; the χ-Fe_5C_2 phase disappeared after 175 hours while the superparamagnetic carbide was present throughout the run. Bulk carbide or oxide phases do not appear to be active species for the FTS; however, this does not eliminate the possibility that a surface carbide or oxide is the active species (VI.7.30,VI.7.31). It is also quite apparent that neither the iron oxide content nor the iron carbide content is related to the deactivation of iron FT catalysts. Both *RJO-168* and *RJO-169* deactivated fairly rapidly over the first 200 hours of synthesis; however, based on XRD analysis, the catalyst used in *RJO-168* oxidized almost completely to Fe_3O_4 while *RJO-169* reduced to a mixture of ϵ'-$Fe_{2.2}C$ and χ-Fe_5C_2. These results do indicate that potassium promotes the carbiding of iron catalysts. This is substantiated by the results of RJO-164, RJO-165 and RJO-166; after 72 hours of synthesis, the iron fraction of carbides was 16%, 70% and 73%, respectively.

VI.7.4. REFERENCES

VI.7.1. Rao, V. U. S., Stiegel, G. J., Cinquegrane, G. J., and Srivastava, R. D., *Fuel Process. Technol.* **30**, 83 (1992).

VI.7.2. Kölbel, H. and Ralek, M., *Catal. Rev.-Sci. Eng.* **21**, 225 (1980).

VI.7.3. Srivastava, R. D., Rao, V. U. S., Cinquegrane, G. and Stiegel, G. J., *Hydrocarbon Process.* **69**, 59 (1990).

VI.7.4. Fox, J. M., III, *Catal. Lett.* **7**, 281 (1990).

VI.7.5. Dry, M. E., *Catal. Lett.* **7**, 241 (1990).

VI.7.6. Dry, M. E., *in Catalysis: Science and Technology* (J. R. Anderson and Boudart, Eds.), Vol 1. Springer-Verlag, New York, 1981.

VI.7.7. Bukur, D. B., Mukesh, D., and Patel, S. A, *Ind. Eng. Chem. Res.* **29**, 194 (1990).

VI.7.8. Bukur, D. B., Lang, X., Mukesh, D., Zimmerman, W. H., Rosynek, M. P. and Li, C., *Ind. Eng. Chem. Res.* **29**, 1588 (1990).

VI.7.9. Le Caër, G., Dubois, J. M., Pijolat, M., Perrichon, V. and Bussière, P., *J. Phys. Chem.* **86**, 4799 (1982).

VI.7.10. Tau, L. M., Borcar, S., Bianchi, D., and Bennett, C. O., *J. Catal.* **87**, 36 (1984).

VI.7.11. Niemantsverdriet, J. W., Flipse, C. F. J., Van Der Kraan, A. M., and Van Loeff, J. J., *Appl. Surf. Sci.* **10**, 302 (1982).

VI.7.12. Amelse, J. A., Butt, J. B., and Schwartz, L. H., *J. Phys. Chem.* **82**, 558 (1978).

VI.7.13. Berry, F., and Smith, M. R., *J. Chem. Soc., Faraday Trans.* 1 **85**, 467 (1989).

VI.7.14. Jung, H., and Thomson, W. J., **J. Catal. 134**, 654 (1992).

VI.7.15. Jung, H., and Thomson, W. J., **J. Catal. 139**, 375 (1993).

VI.7.16. McCartney, J. T., Hofer, L. J. E., Seligman, B., Lecky, J. A., Peebles, W. C., and Anderson, R. B., *J. Phys. Chem.* **57**, 730 (1953).

VI.7.17. Huang, C.-S., Xu, L., and Davis, B., *Fuel Sci. & Technol. Int.* **11**, 639 (1993).

VI.7.18. Huang, C.-S., Gunguly, B., Huffman, G. P., Huggins, F. E., and Davis, B. H., *Fuel Sci. & Technol. Int.* **11**, 1289 (1993).

VI.7.19. Soled, S., Iglesia, E., and Fiato, R. A., *Catal. Lett.* **7**, 271 (1990).

VI.7.20. Bukur, D. B., Lang, X., Koranne, M., and Nowicki, L., Proc. Coal Gasification and Gas Conversion Contractors' Review Conference, Sept., 1993, Pittsburgh, p. 943.

VI.7.21. Itoh, H., Hosaka, H., Ono, T., and Kikuchi, E., *Appl. Catal.* **40**, 53 (1988).

VI.7.22. Lox, E. S., Marin, G. B., De Grave, E., and Bussière, P., *Appl. Catal.*, **40**, 197 (1988).

VI.7.23. Tau, L.-M., Dabbagh, H. A., Davis, B. H., *Energy & Fuels* **4**, 94 (1990).

VI.7.24. Dry, M. E., Shingles, T., Boshoff, L. J., and Oosthuizen, G. J., *J. Catal.*, **15**, 190 (1969).

VI.7.25. Donnelly, T. J., Yates, I. C., and Satterfield, C. N., *Energy & Fuels* **2**, 734 (1988).

VI.7.26. Sault, A. G., and Datye, A. K., *J. Catal.* **140**, 136 (1993).

VI.7.27. Vogler, G. L., Jiang, X. Z., Dumesic, J. A., and Madon, R. J., *J. Catal.*, **89**, 116 (1984).

VI.7.28. Fischer, F., and Tropsch, H., *Brenstoff-Chem.* **7**, 97 (1926).

VI.7.29. Reymond, J. P., Mériaudeau, P., and Teichner, S. J., *J. Catal.* **75**, 39 (1982).

VI.7.30. Biloen, P., Helle, J. N., and Sachtler, W. M. H., *J. Catal.* **58**, 95 (1979).

VI.7.31. Niemantsverdriet, J. W., Flipse, C. F. J., Van Der Kraan, and Van Loef, J. J., *Appl. Surf. Sci.* **10**, 302 (1982).

Table VI.7.1

Catalyst Compositions in Atomic %, X/(Fe + X)

Run Number	Composition
RJO-168	100Fe
RJO-169	100Fe/0.71K
RJO-137	100Fe/0.71K/4.4Si
RJO-163	100Fe/0.71K/2.6Cu/4.4Si
RJO-164	100Fe/0.71K/4.4Al
RJO-165	100Fe/2.8K/4.4Al
RJO-166	100Fe/7.0K/4.4Al

Table VI.7.2

Catalyst Characterization for RJO-168

Condition	Time, Hr.	Surface Area, m^2/g	Pore Volume, cm^3/g	Pore Diameter, Å	XRD
CO Pretreatment	2.17	19	0.15	320	M
	5.75				M, χ, ϵ'
	10				M, χ, ϵ'
	26	32	0.071	90	M, χ, ϵ'
Synthesis	2				M, χ, ϵ'
	24				M, χ, ϵ'
	48				M, χ, ϵ'
	72	31	0.46	59	M, χ, ϵ'
	122				M, χ, ϵ'
	171				M, χ, ϵ'
	216				M, χ, ϵ'
	337	44	0.25	230	M, χ, ϵ'

M = Fe_3O_4
χ = χ-Fe_5C_2
ϵ' = ϵ'-$Fe_{2.2}C$

Table VI.7.3

Catalyst Characterization for RJO-169

Condition	Time, Hr.	Surface Area, m^2/g	Pore Volume, cm^3/g	Pore Diameter, Å	XRD
CO Pretreatment	2.25	21	0.20	370	M
	7				M
	26.75	29	0.068	90	M, ϵ', χ
Synthesis	4.25	31	0.065		M, ϵ', χ
	26	20	0.31		M, ϵ', χ
	47				M, ϵ', χ
	73				ϵ', χ, M
	100				ϵ', χ, M
	122				ϵ', χ, M
	146	49	0.41	330	ϵ', χ, M

M = Fe_3O_4
χ = χ-Fe_5C_2
ϵ' = ϵ'-$Fe_{2.2}C$

Table VI.7.4

Catalyst Characterization for RJO-137

Condition	Time, Hr.	Surface Area, m^2/g	Pore Volume, cm^3/g	Pore Diameter, Å	Mössbauer Phase (%Fe)	XRD
CO Pretreatment	7.75	120	0.22	75	S(66), M(34)	M
	27.5	70	0.25	140	SC(39), M(37), χ(24)	M, χ, ϵ'
Synthesis	4.5	77	0.32	170		M, χ, ϵ'
	28				SC(50), χ(34), M(16)	M, χ, ϵ'
	50	84	0.40	190		M, χ, ϵ'
	72	73	0.32	170	SC(41), χ(34), M(26)	M, χ, ϵ'
	103					M, χ, ϵ'
	124					M, χ
	148	77	0.48	250		M, χ
	175				SC(41), M(32), χ(27)	M, χ, ϵ'
	191					M, χ, ϵ'
	320				M(83), SC(17)	M
	461	87	0.43	200		M, χ, ϵ'

S = superparamagnetic oxide
SC = superparamagnetic carbide
M = $Fe_3O\underline{124}$
χ = Fe_5C_2
ϵ' = ϵ'-$Fe_{2.2}C$

Table VI.7.5

Catalyst Characterization for RJO-163

Condition	Time, Hr.	Surface Area, m^2/g	Pore Volume, cm^3/g	Pore Diameter, Å	XRD
CO Pretreatment	3.5	62	0.20	130	M
	7.0				M, χ, ϵ'
	26.5	66	0.24	150	M, χ, ϵ'
Synthesis	4.0				M, χ, ϵ'
	26				M, χ, ϵ'
	50	60	0.32	215	M, χ, ϵ'
	80				M, χ, ϵ'
	124				M, χ, ϵ'
	194	90	0.44	200	M, χ, ϵ'
	292	84	0.30	144	M, χ, ϵ'

M = Fe_3O_4
χ = χ-Fe_5C_2
ϵ' = ϵ'-$Fe_{2.2}C$

Table VI.7.6

Catalyst Characterization for RJO-164

Condition	Time, Hr.	Surface Area, m^2/g	Pore Volume, cm^3/g	Pore Diameter, Å	Mössbauer Phase (%Fe)	XRD
CO Pretreatment	3.17	68	0.21	120		M
	7					M
	26.8	70	0.30	170	χ(70), M(24), SC(6)	M, χ, ϵ'
Synthesis	4	77	0.34			M, χ, ϵ'
	26					M, χ
	48					M, χ, ϵ'
	72	104	0.43	170	M(84), SC(16)	M, χ, ϵ'

S = superparamagnetic oxide
SC = superparamagnetic carbide
M = Fe_3O_4
χ = Fe_5C_2
ϵ' = ϵ'-$Fe_{2.2}C$

Table VI.7.7

Catalyst Characterization for RJO-165

Condition	Time, Hr.	Surface Area, m^2/g	Pore Volume, cm^3/g	Pore Diameter, Å	Mössbauer Phase (%Fe)	XRD
CO Pretreatment	3.17	49	0.21	170		M
	7					M
	26.8	58	0.45	310	M(62), χ(34), SC(4)	M, χ
Synthesis	4	60	0.35			M, χ, ϵ'
	26					M, χ, ϵ'
	48					M, χ, ϵ'
	72	41	0.18	180	M(43), ϵ'(41), SC(10), χ(6)	M, χ, ϵ'

S = superparamagnetic oxide
SC = superparamagnetic carbide
M = Fe_3O_4
χ = Fe_5C_2
ϵ' = ϵ'-$Fe_{2.2}C$

Table VI.7.8

Catalyst Characterization for RJO-166

Condition	Time, Hr.	Surface Area, m^2/g	Pore Volume, cm^3/g	Pore Diameter, Å	Mössbauer Phase (%Fe)	XRD
CO Pretreatment	3.17	35	0.169	190		M
	7					M, χ
	26.8	< 3	0.085	--	M(34), χ(34), ϵ'(23), SC(9)	M, χ, ϵ'
Synthesis	4					M, χ, ϵ'
	26					M, χ, ϵ'
	48					M, χ, ϵ'
	72	< 3	0.085	--	M(43), ϵ'(41), SC(10), χ(6)	M, χ, ϵ'

S = superparamagnetic oxide
SC = superparamagnetic carbide
M = Fe_3O_4
χ = Fe_5C_2
ϵ' = ϵ'-$Fe_{2.2}C$

Table VI.7.9

Activity and Product Selectivity of Catalysts

Run No.	CO Conv.[a]	$C_2=$[b]	$C_3=$[c]	$C_4=$[d]	1-$C_4=$[e]	Kapp[f]	CO_2/CO[g]	CH_4%[h]	HC[i]	C_3+[j]
RJO-168	84	0.14	0.61	0.74	0.44	9.6	0.47	7.0	165	141
RJO-169	82	0.69	0.84	0.87	0.96	24	0.49	4.0	155	141
RJO-137	84	0.09	0.56	0.67	0.41	26	0.46	8.0	168	140
RJO-163	85	0.08	0.45	0.65	0.33	22	0.50	9.0	155	128
RJO-164	84	0.28	0.79	0.80	0.70		0.51	6.4	152	130

a. %
b. C_2 alkene fraction
c. C_3 alkene fraction
d. C_4 alkene fraction
e. 1-butene fraction of total butenes
f. $K_{app} = ([H_2][CO_2])/([CO][H_2O])$
g. CO_2 selectivity
h. methane selectivity
i. total hydrocarbon production, g/m^3 of CO + H_2
j. C_3+ hydrocarbon production, g/m^3 of CO + H_2

Table VI.7.10

ASF Parameters for Catalysts

Catalyst	TOS, Hr.	CO Conv., %	α_1	α_2	ζ
RJO-168	216	48	0.73[a]		
RJO-169	145	46	0.77[a]	0.81[b]	
RJO-137	383	85	0.65[c]	0.80[c]	12.5[c]
RJO-163	290	74	0.65[c]	0.86[c]	10.3[c]

a. Determined from measured slope between C_3 and C_{10}.
b. Determined from measured slope between C_{10} and C_{20}.
C. Determined by the method of Satterfield described in reference 25.

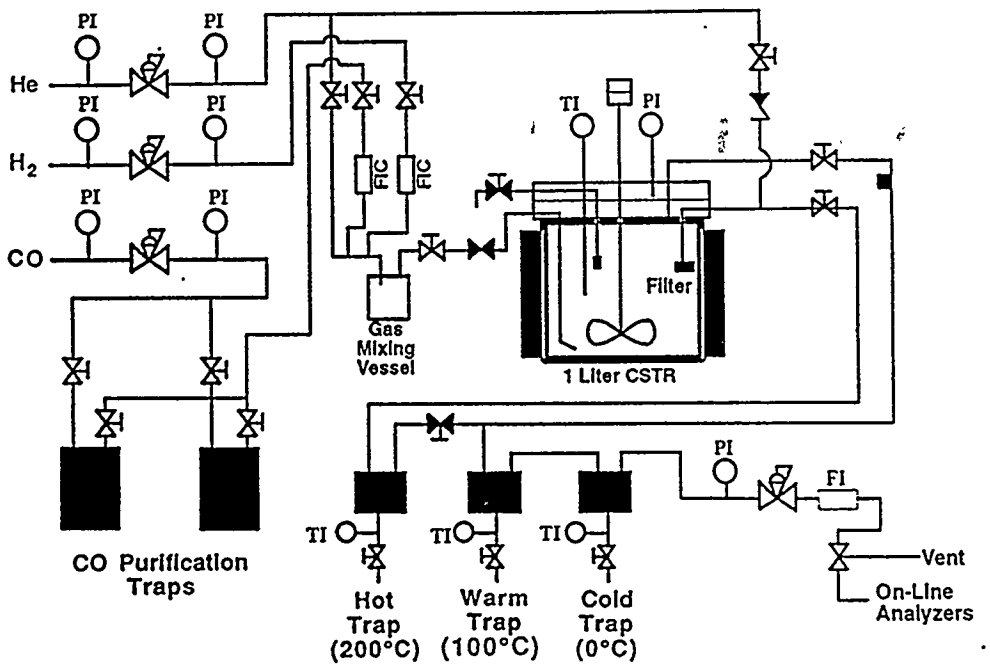

Figure VI.7.1. Schematic of the one liter CSTR unit showing trap configurations.

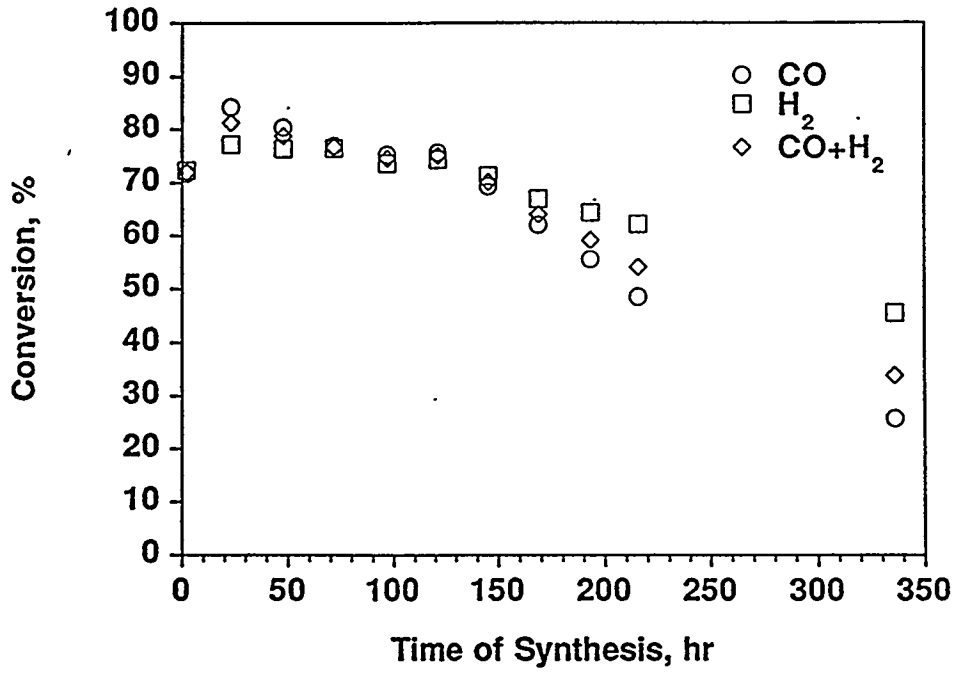

Figure VI.7.2. Conversion data as a function of time of synthesis for RJO-168.

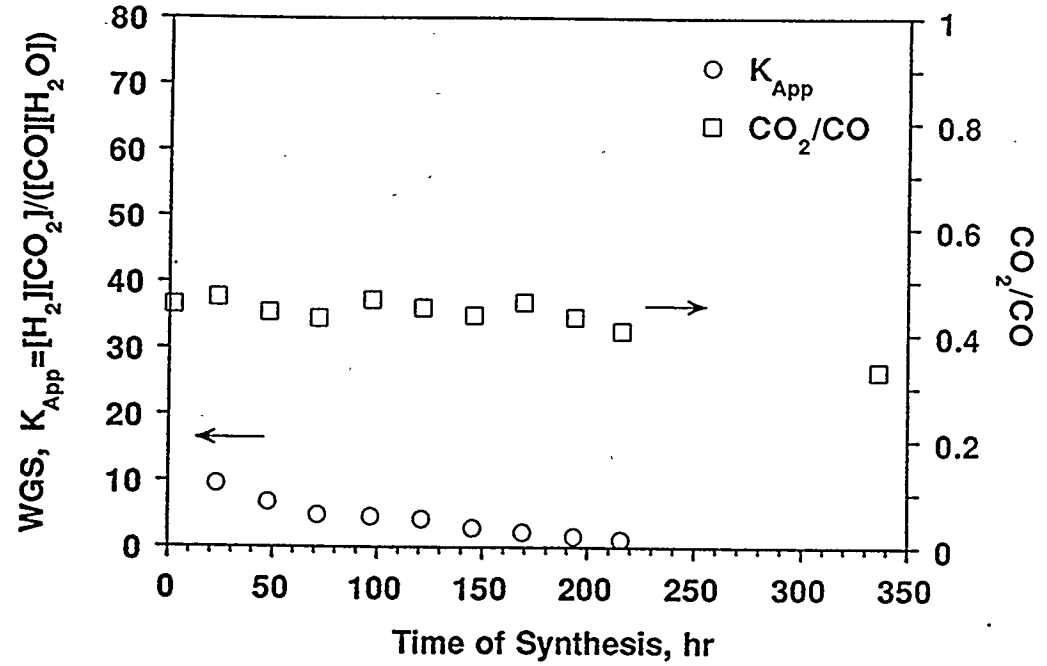

Figure VI.7.3. Water-gas shift reaction coefficient and CO_2/CO ratio as a function of time of synthesis for RJO-168.

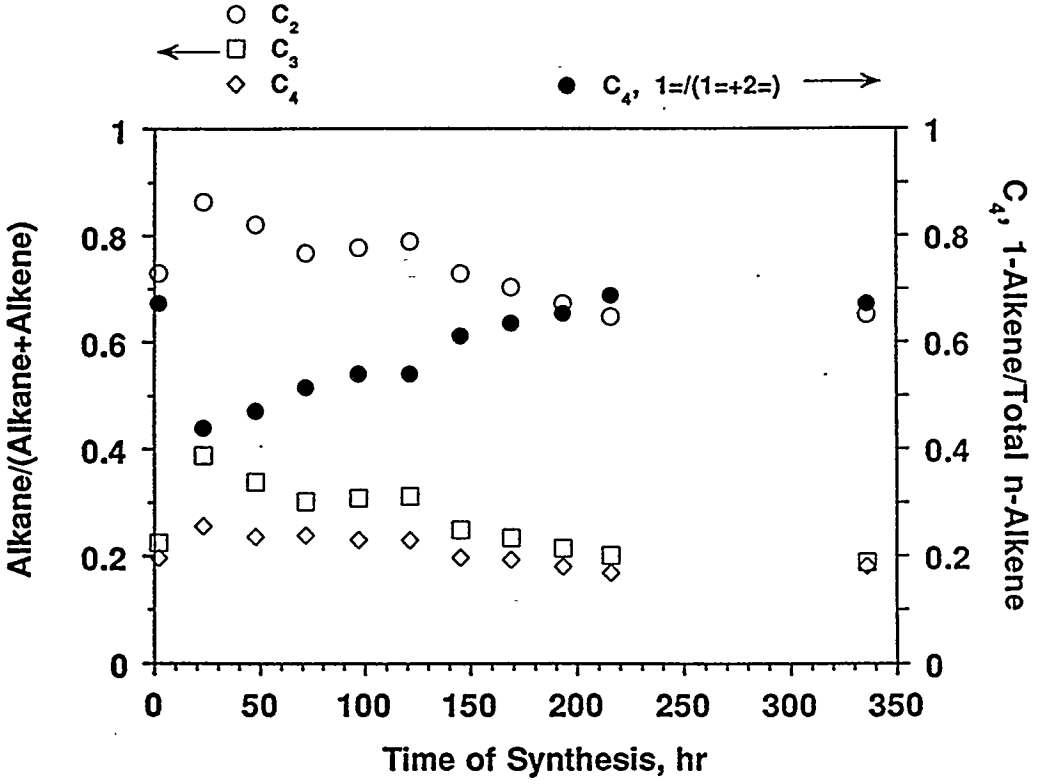

Figure VI.7.4. C_2, C_3 and C_4 alkane/alkene selectivity and 1-butene selectivity for RJO-168.

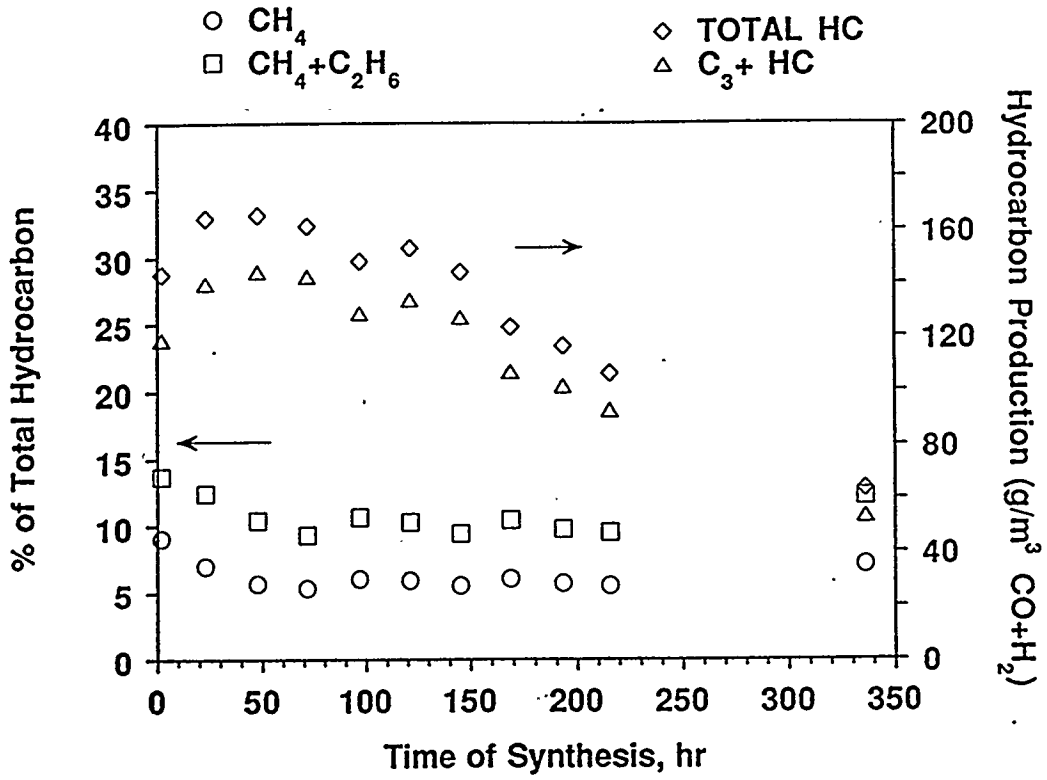

Figure VI.7.5. Total hydrocarbon and C_3+ hydrocarbon production and methane and ethane selectivity as a function of time of synthesis for RJO-168.

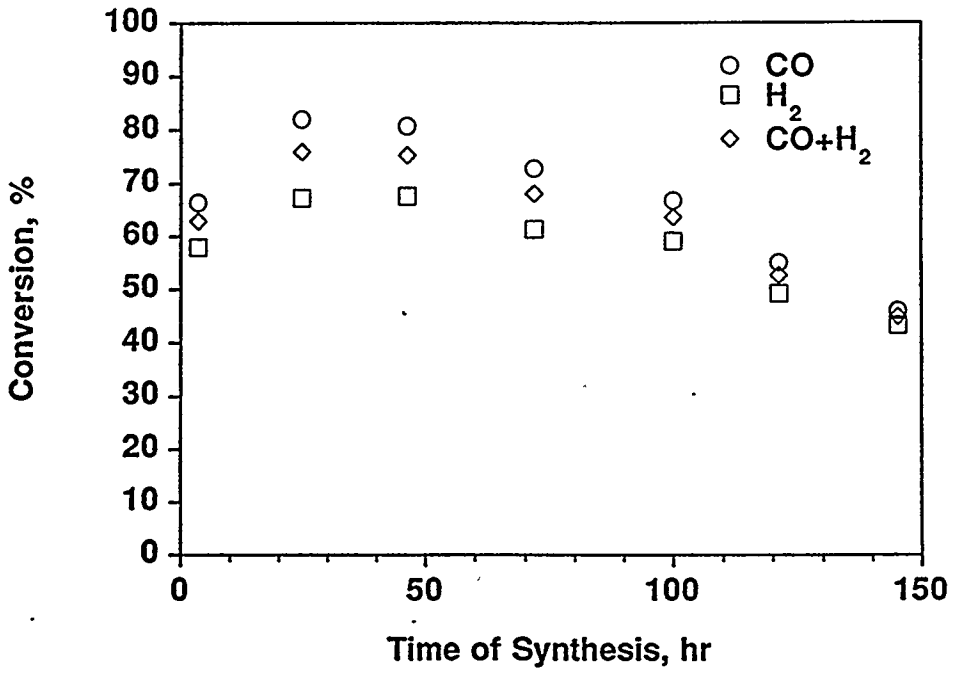

Figure VI.7.6. Conversion data for as a function of time of synthesis for RJO-169.

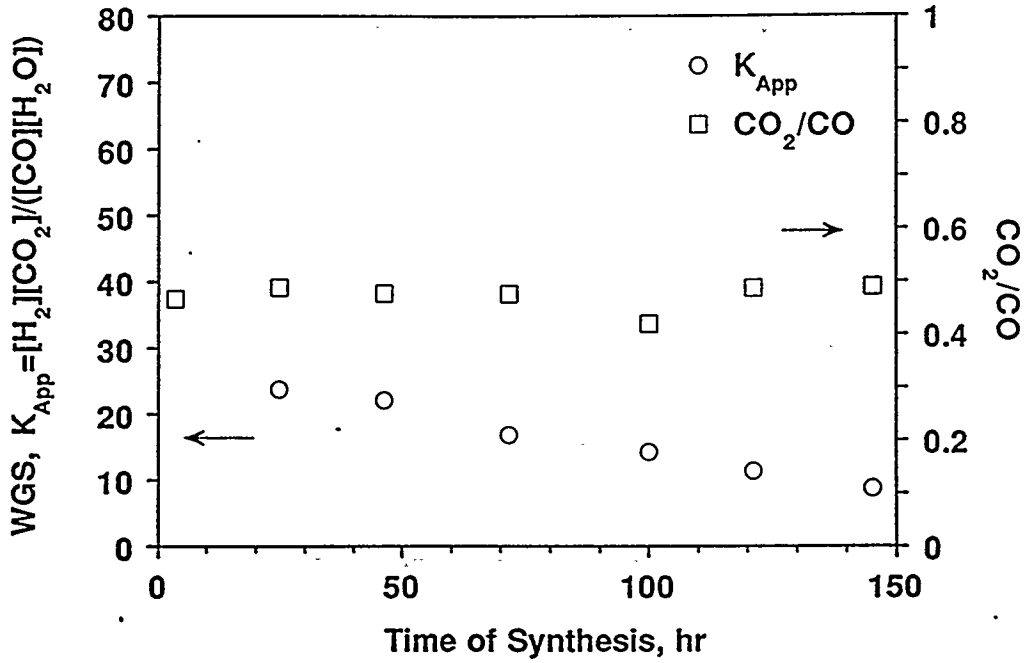

Figure VI.7.7. Water-gas shift reaction coefficient and CO_2/CO ratio as a function of time of synthesis for RJO-169.

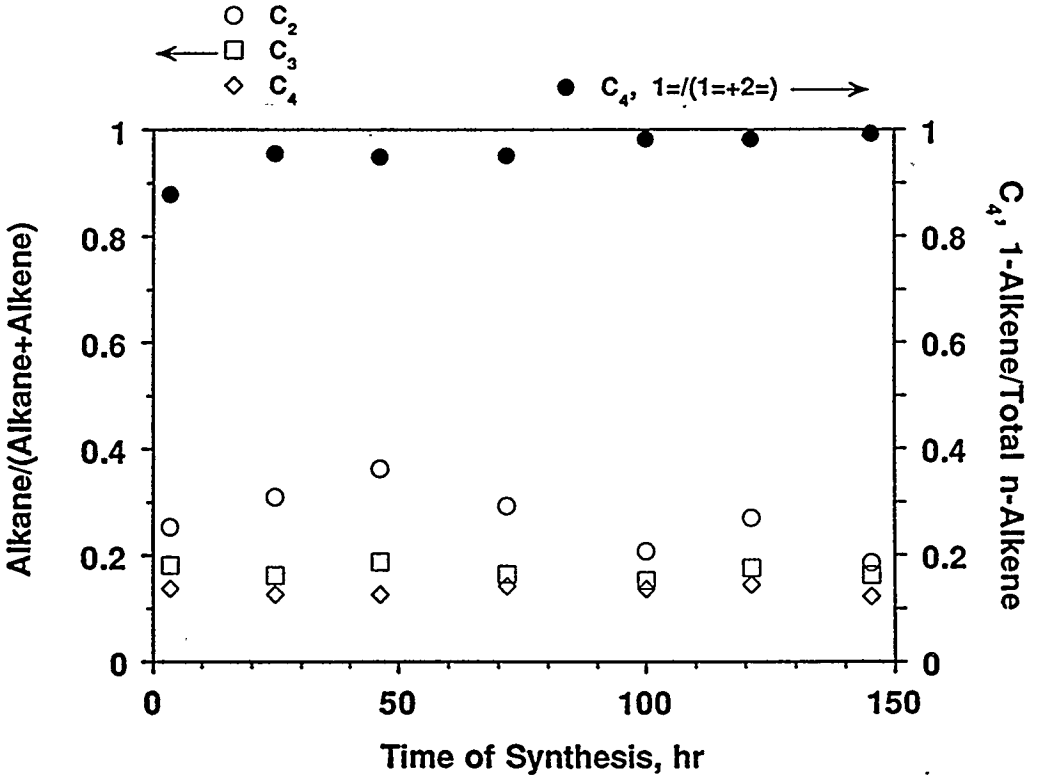

Figure VI.7.8. C_2, C_3 and C_4 alkane/alkene selectivity and 1-butene selectivity for RJO-169.

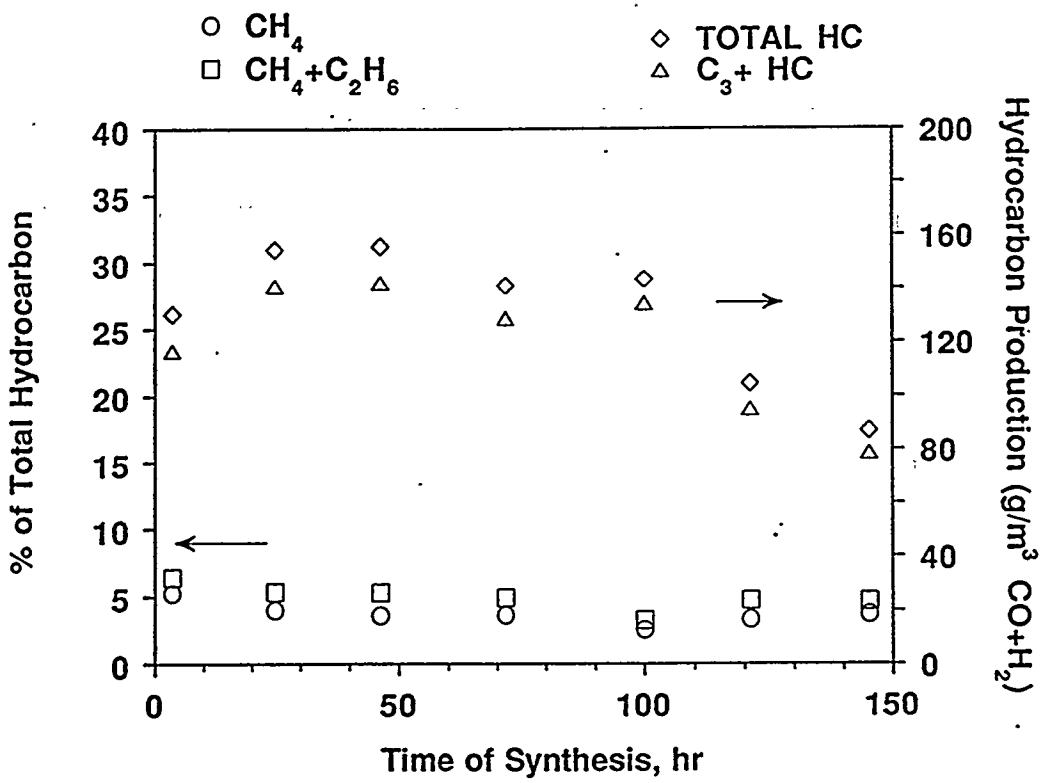

Figure VI.7.9. Total hydrocarbon and C_3+ hydrocarbon production and methane and ethane selectivity as a function of time of synthesis for RJO-169.

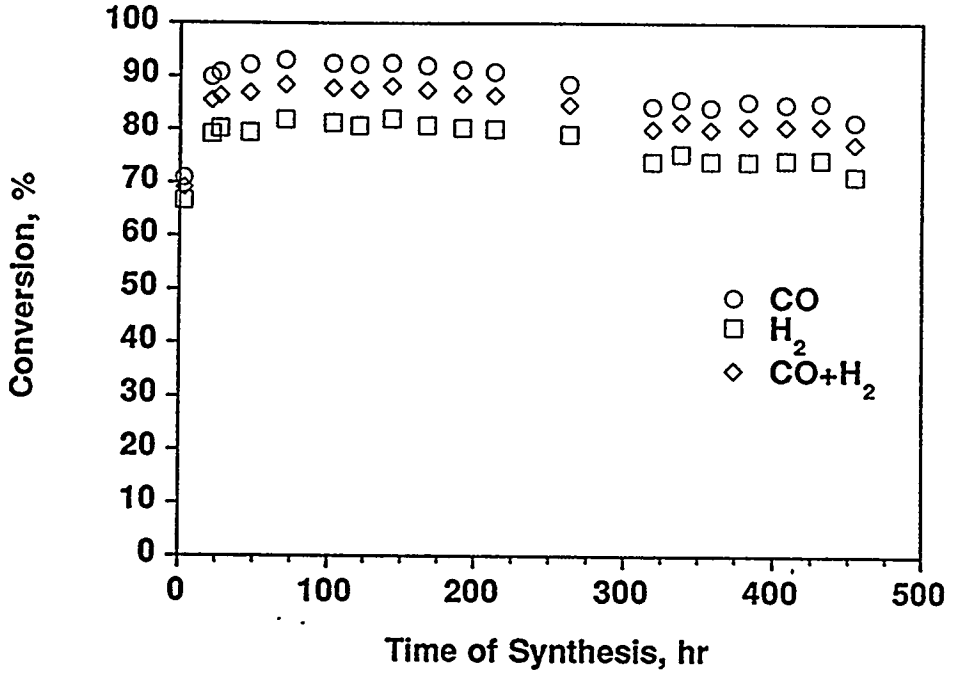

Figure VI.7.10. Conversion data as a function of time of synthesis for RJO-137.

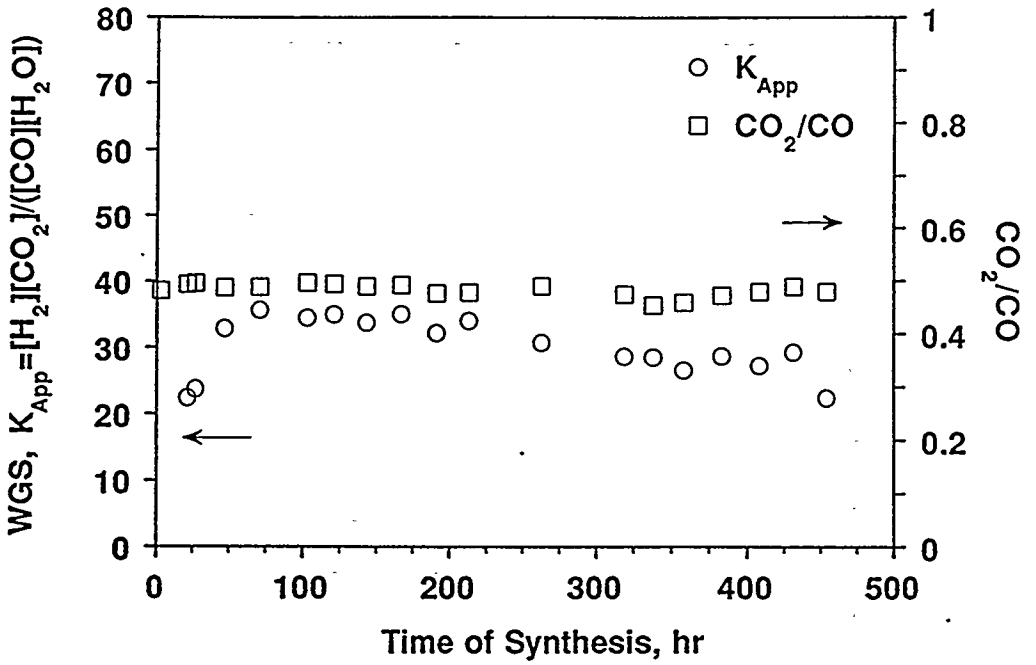

Figure VI.7.11. Water-gas shift reaction coefficient and CO_2/CO ratio as a function of time of synthesis for RJO-137.

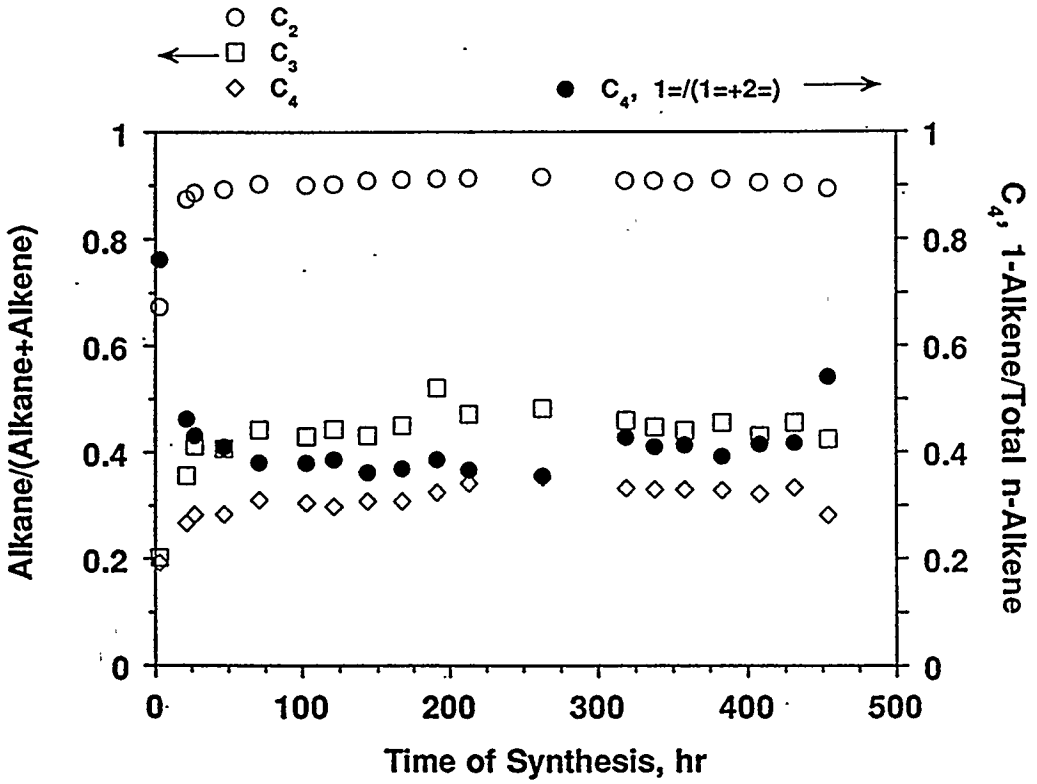

Figure VI.7.12. C_2, C_3 and C_4 alkane/alkene selectivity and 1-butene selectivity for RJO-137.

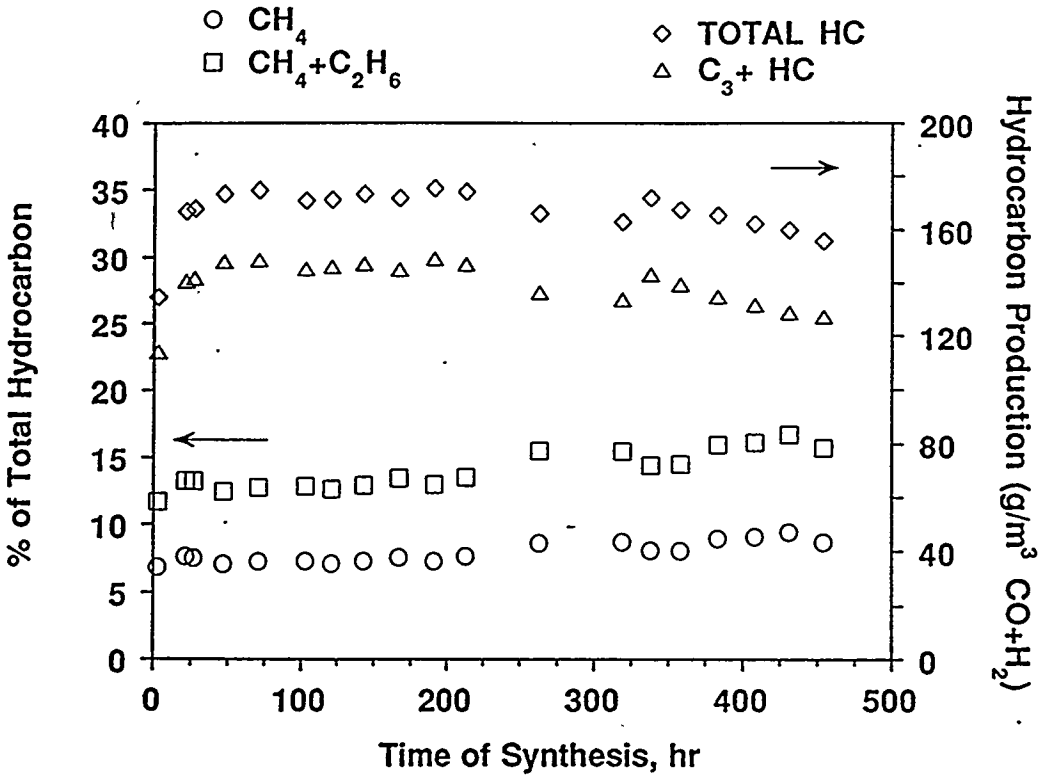

Figure VI.7.13. Total hydrocarbon and C_3+ hydrocarbon production and methane and ethane selectivity as a function of time of synthesis for RJO-137.

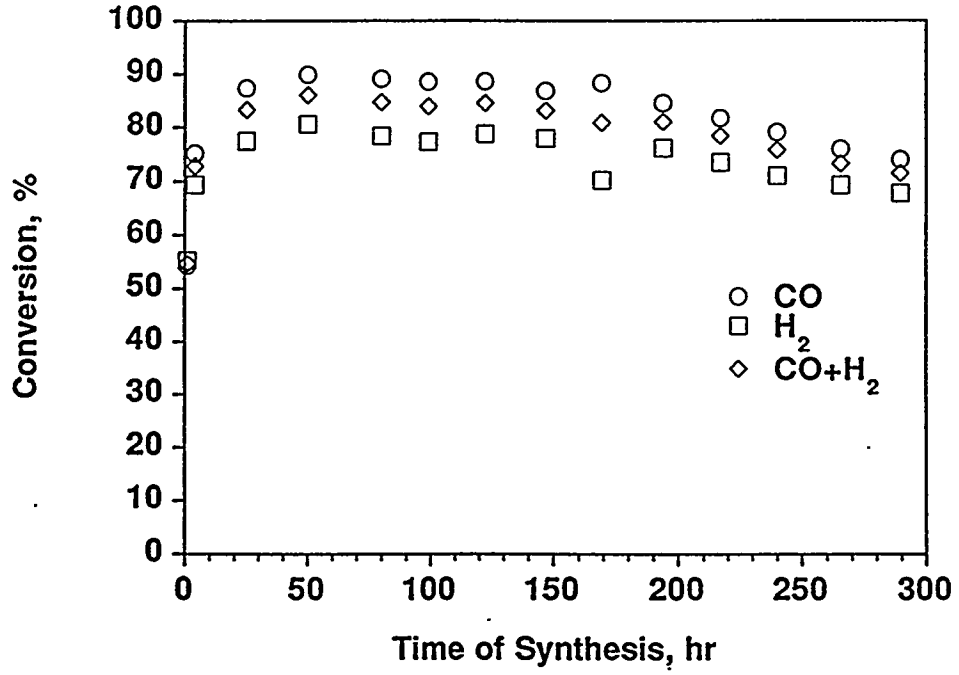

Figure VI.7.14. Conversion data as a function of time of synthesis for RJO-163.

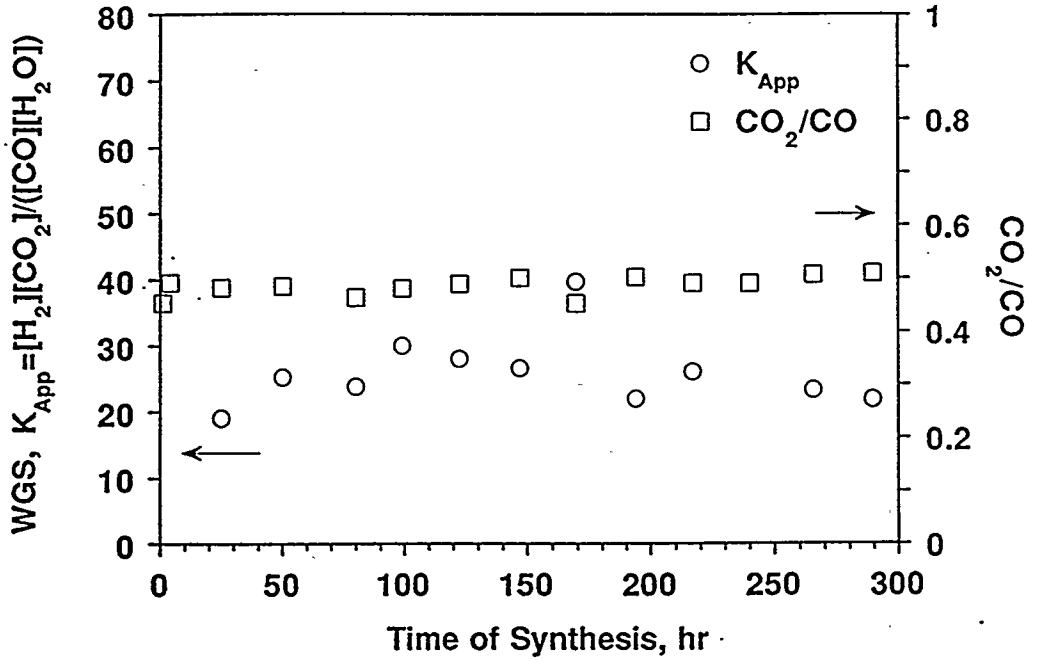

Figure VI.7.15. Water-gas shift reaction coefficient and CO_2/CO ratio as a function of time of synthesis for RJO-163.

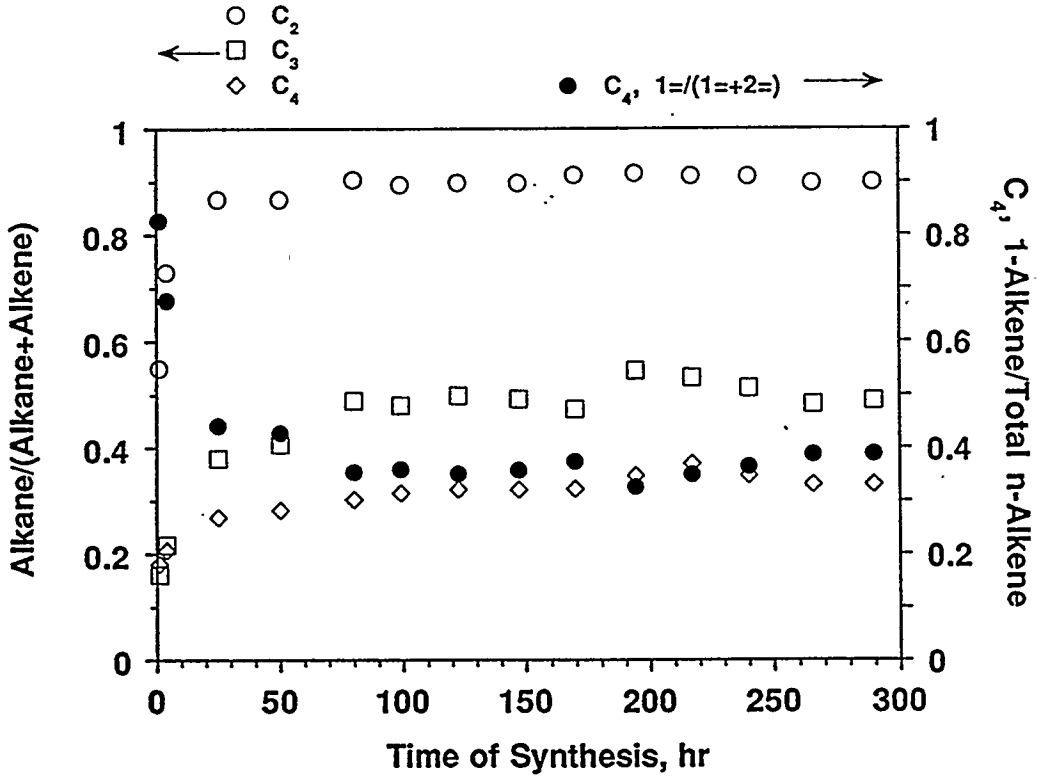

Figure VI.7.16. C_2, C_3 and C_4 alkane/alkene selectivity and 1-butene selectivity for RJO-163.

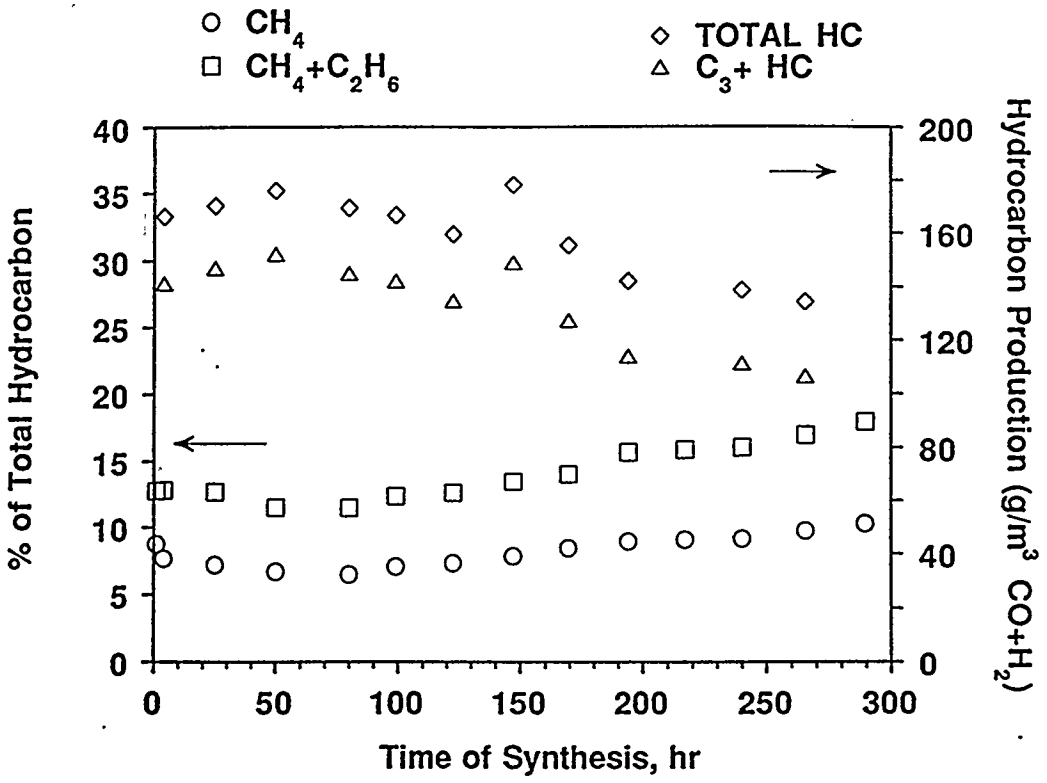

Figure VI.7.17. Total hydrocarbon and C_3+ hydrocarbon production and methane and ethane selectivity as a function of time of synthesis for RJO-163.

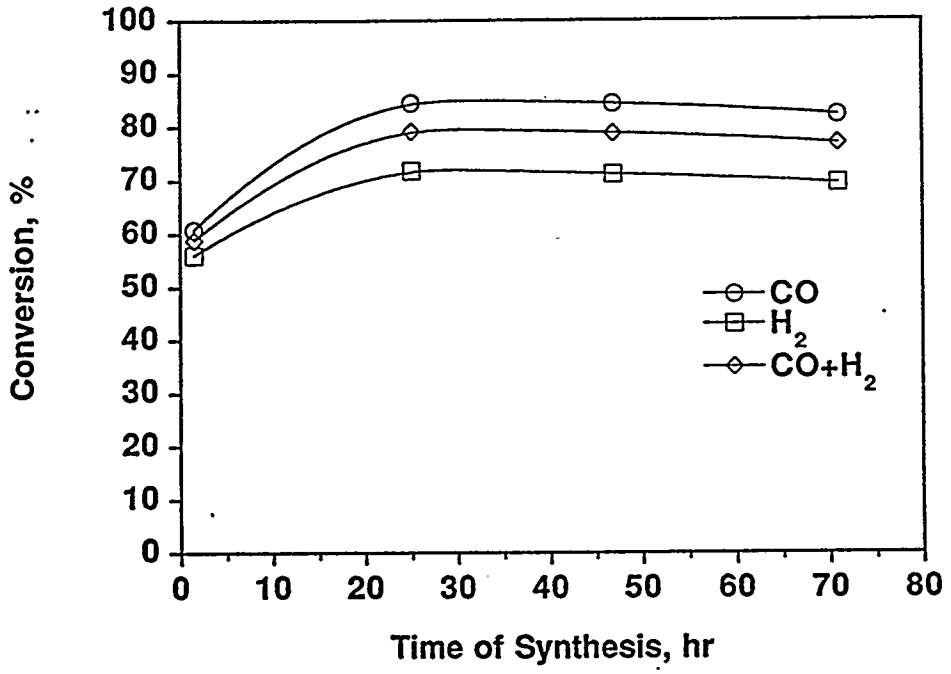

Figure VI.7.18. Conversion data as a function of time of synthesis for RJO-164.

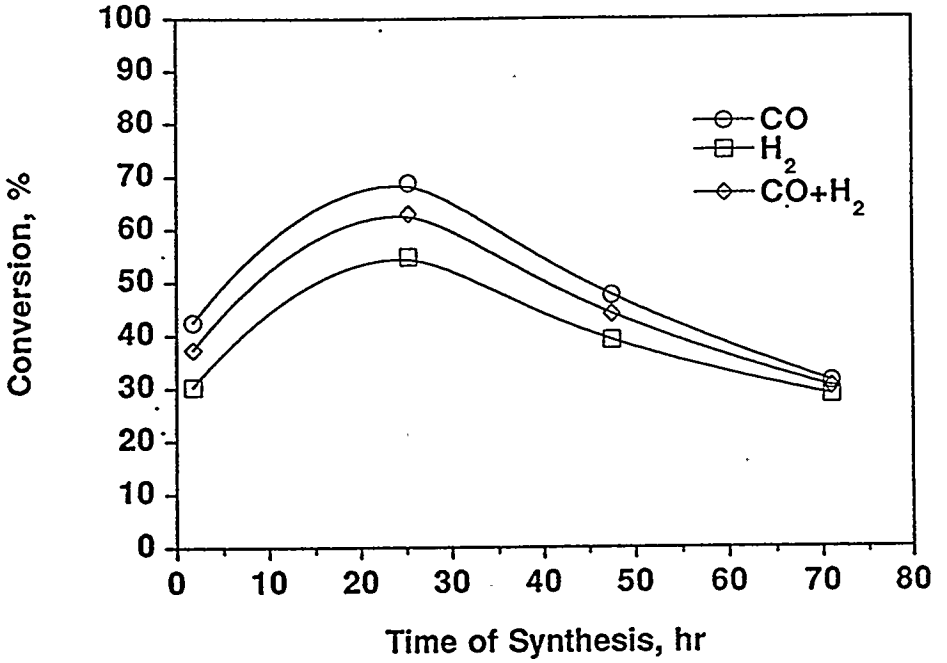

Figure VI.7.19. Conversion data as a function of time of synthesis for RJO-165.

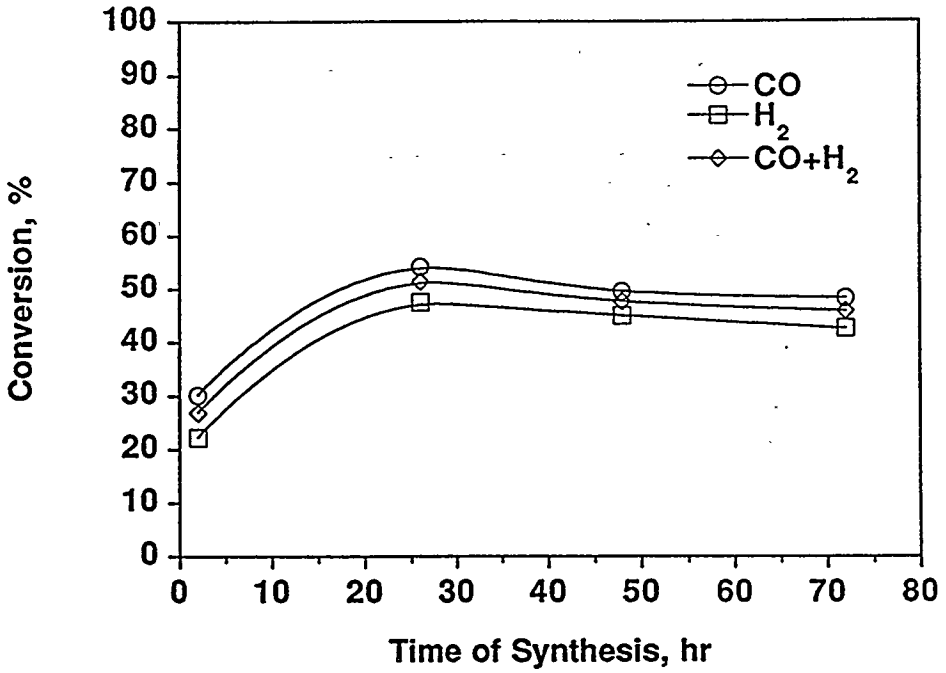

Figure VI.7.20. Conversion data as a function of time of synthesis for RJO-166.

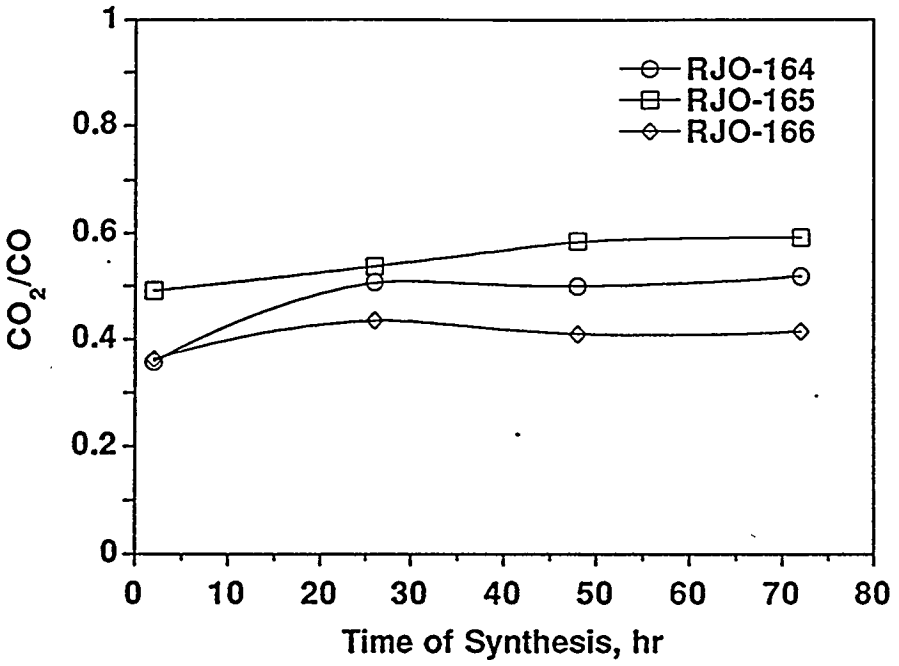

Figure VI.7.21. CO_2 selectivity in terms of CO_2/CO ratio as a function of time of synthesis for RJO-164, RJO-165 and RJO-166.

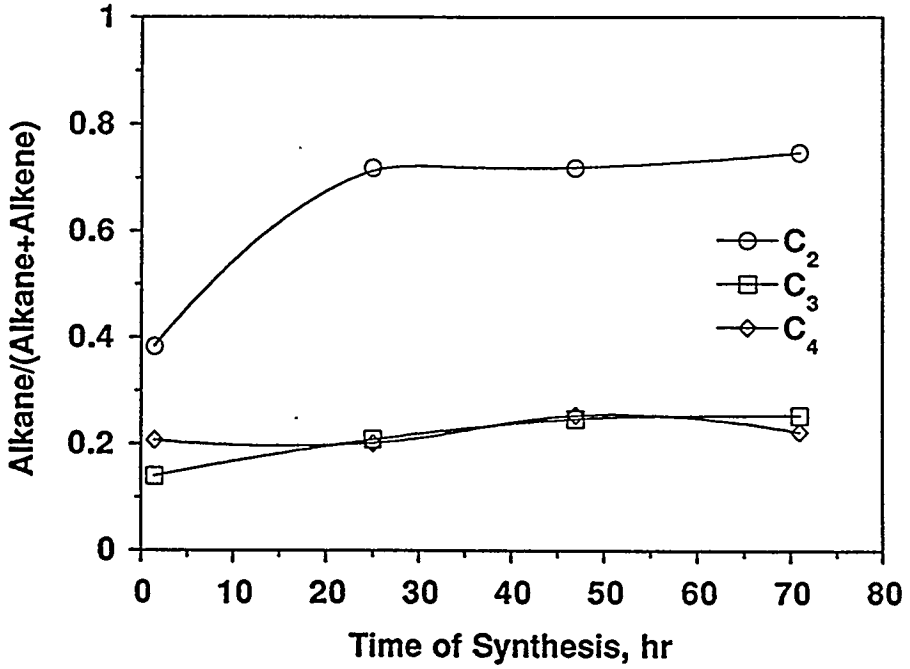

Figure VI.7.22. C_2, C_3 and C_4 alkane/alkene selectivity as a function of time of synthesis for RJO-164.

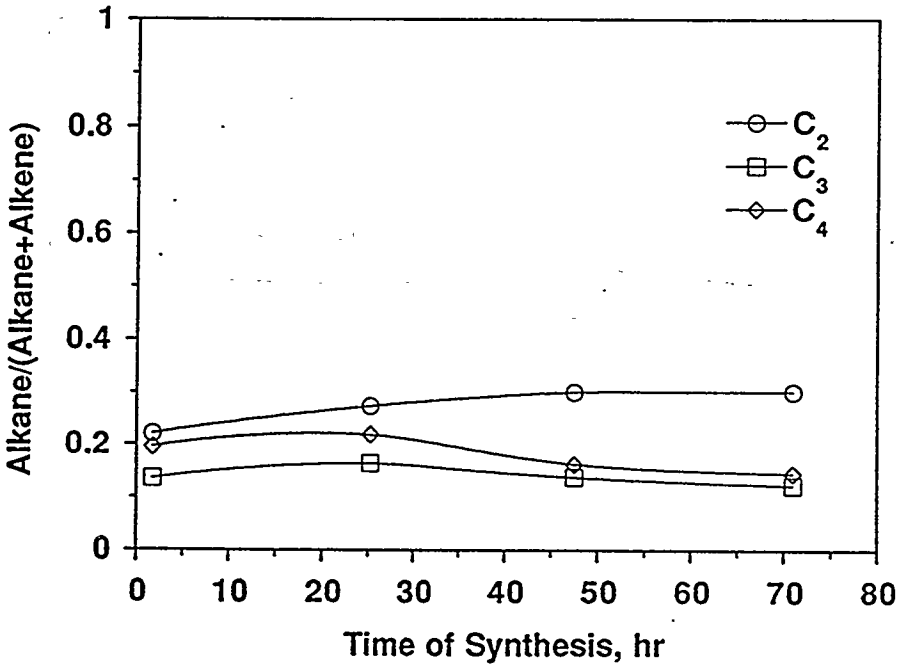

Figure VI.7.23. C_2, C_3 and C_4 alkane/alkene selectivity as a function of time of synthesis for RJO-165.

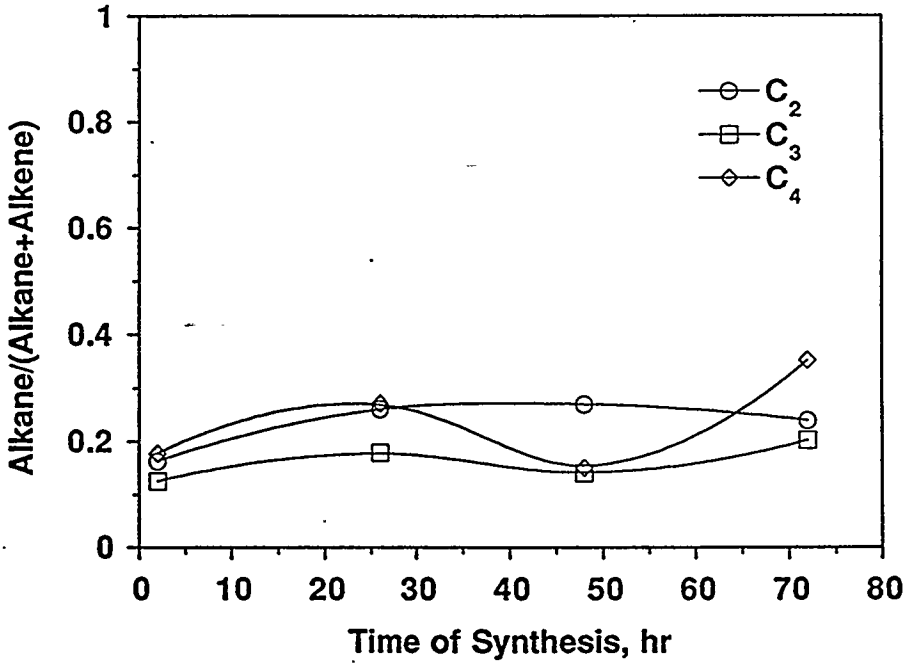

Figure VI.7.24. C_2, C_3 and C_4 alkane/alkene selectivity as a function of time of synthesis for RJO-166.

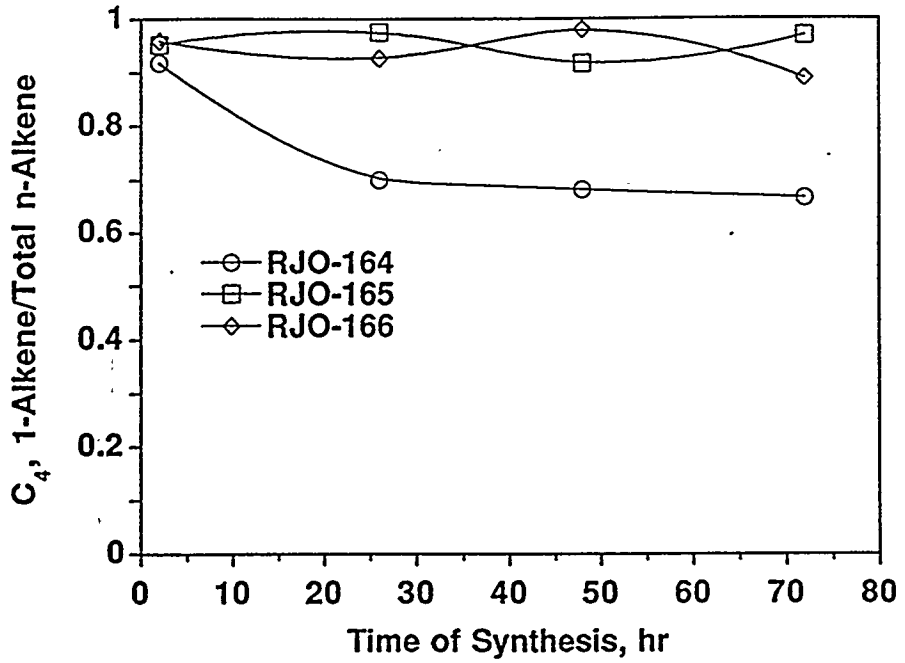

Figure VI.7.25. Fraction of 1-butene in total C_4 alkene fraction as a function of time of synthesis.

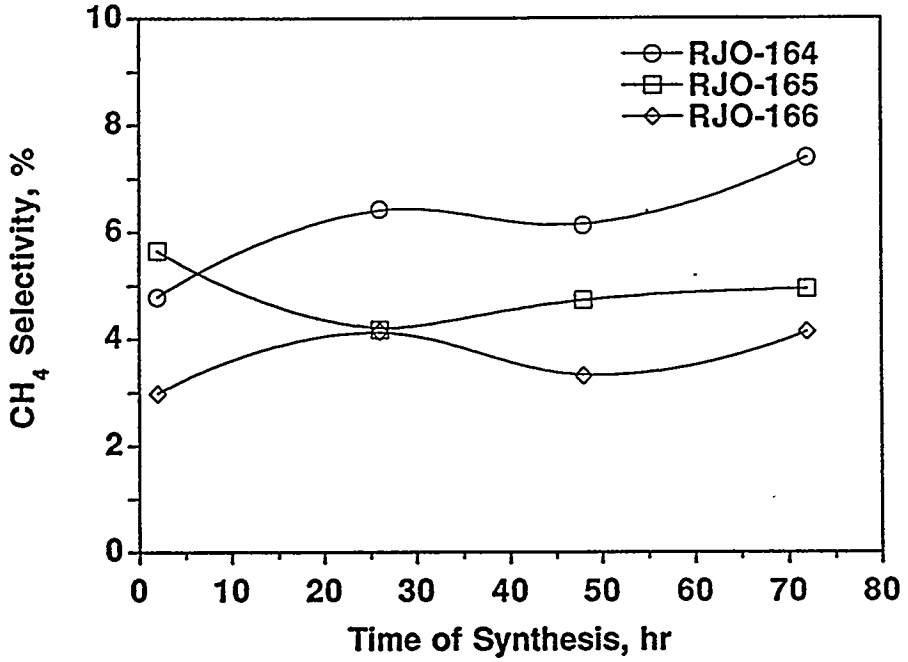

Figure VI.7.26. Methane selectivity as a function of time of synthesis for RJO-164, RJO-165 and RJO-166.

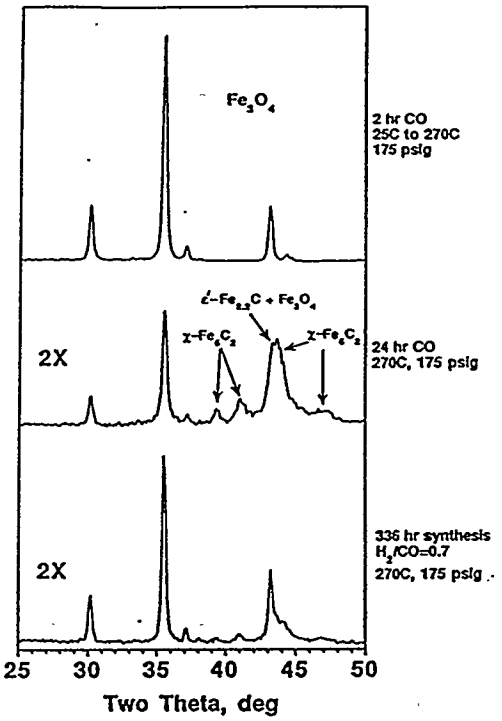

Figure VI.7.27. X-ray diffractograms of unpromoted iron oxyhydroxide catalyst, RJO-168, following the temperature ramp from 25°C to 270°C under CO, following 24 hr at CO pretreatment conditions and 336 hr at synthesis conditions.

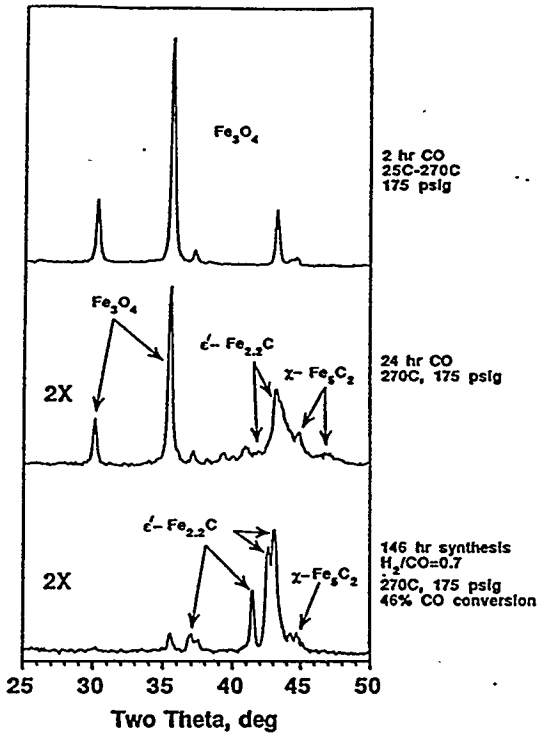

Figure VI.7.28. X-ray diffractograms of iron oxyhydroxide catalyst promoted with 0.71 at.% potassium, RJO-169, following the temperature ramp from 25°C to 270°C under CO, following 24 hr at CO pretreatment conditions and 146 hr at synthesis conditions.

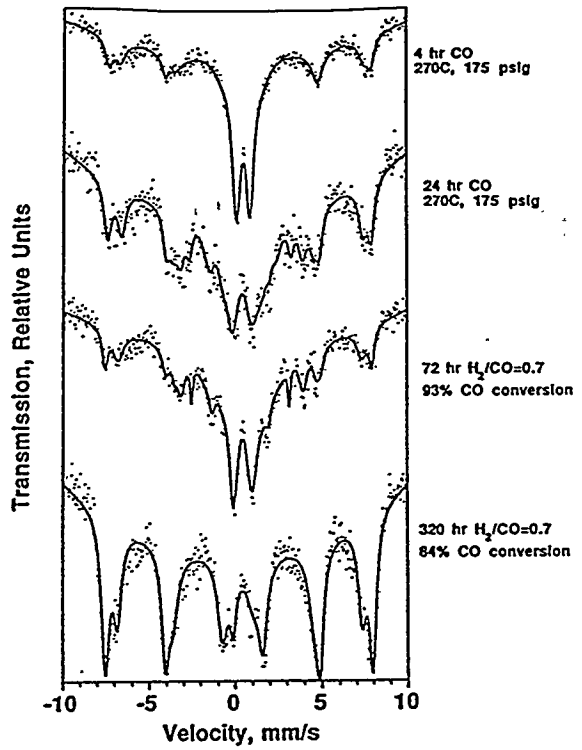

Figure VI.7.29. Mössbauer spectra of iron oxyhydroxide catalyst promoted with 0.71 at.% potassium and 4.4 at.% silicon, RJO-137, following the temperature ramp from 25°C to 270°C under CO, following 24 hr at CO pretreatment conditions, following 72 hr and 336 hr at synthesis conditions.

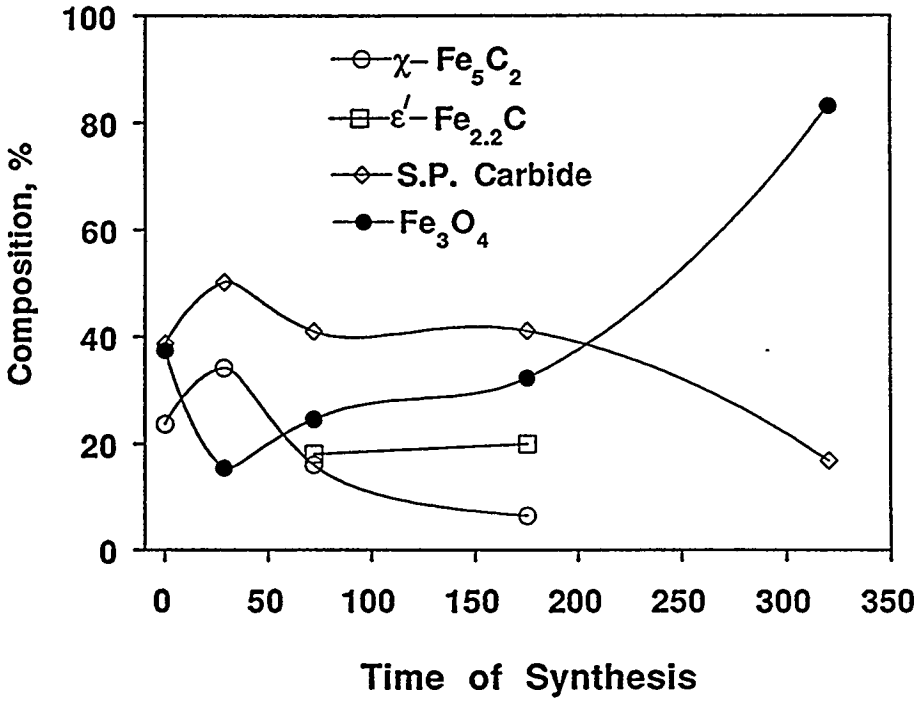

Figure VI.7.30. Composition of iron oxyhydroxide catalyst promoted with 0.71 at.% potassium and 4.4 at.% silicon, RJO-137, as a function of time of synthesis. Composition given as %Fe from Mössbauer results.

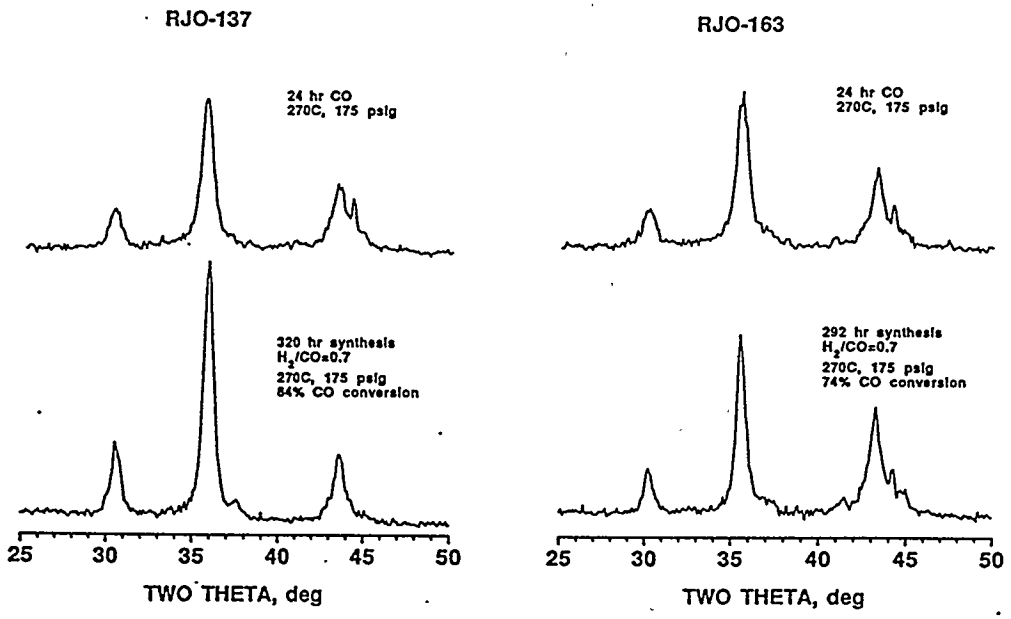

Figure VI.7.31. X-ray diffractograms of RJO-137 and RJO-163 following pretreatment and 320 hr and 292 hr of synthesis, respectively.

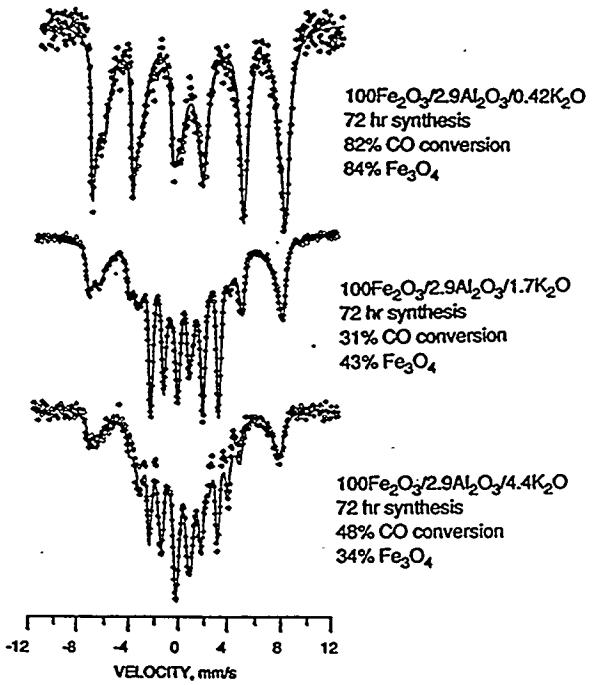

Figure VI.7.32. Mössbauer spectra of iron oxyhydroxide catalyst promoted with 4.4 at.% aluminum and 0.71, 2.8 and 7.0 at.% potassium, RJO-164, RJO-165 and RJO-166, respectively, following 72 hr at synthesis conditions.

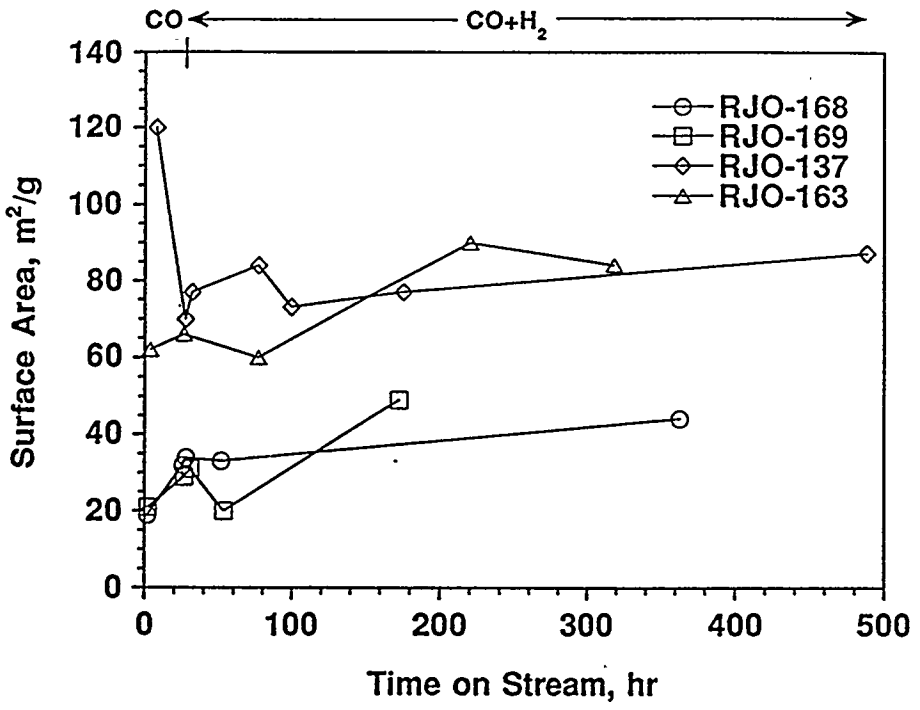

Figure VI.7.33. BET surface area as a function of time on stream for RJO-168, RJO-169, RJO-137 and RJO-163.

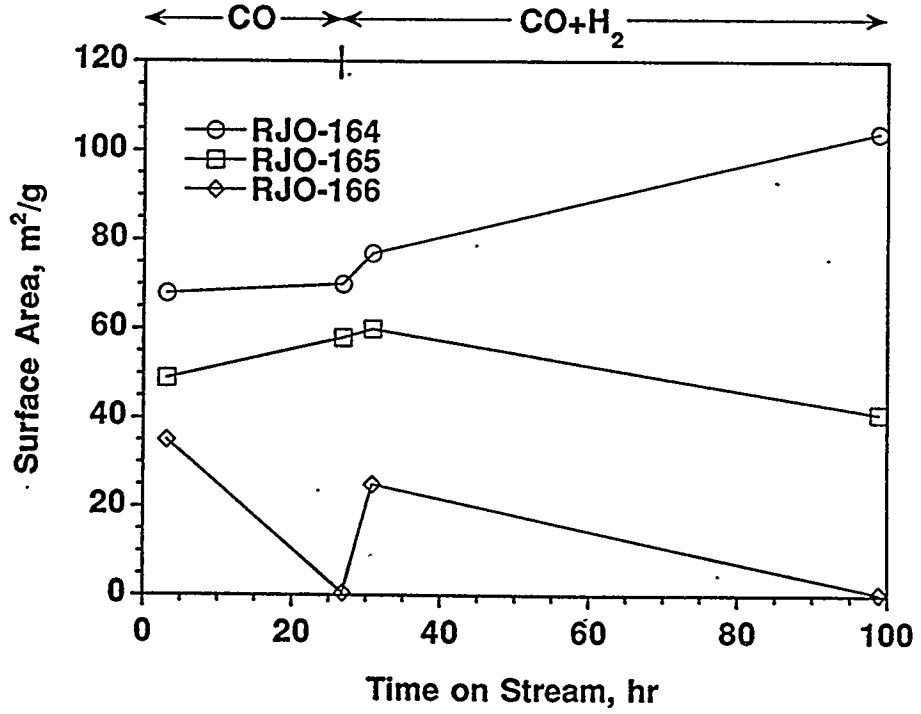

Figure VI.7.34. BET surface area as a function of time on stream for RJO-164, RJO-165 and RJO-166.

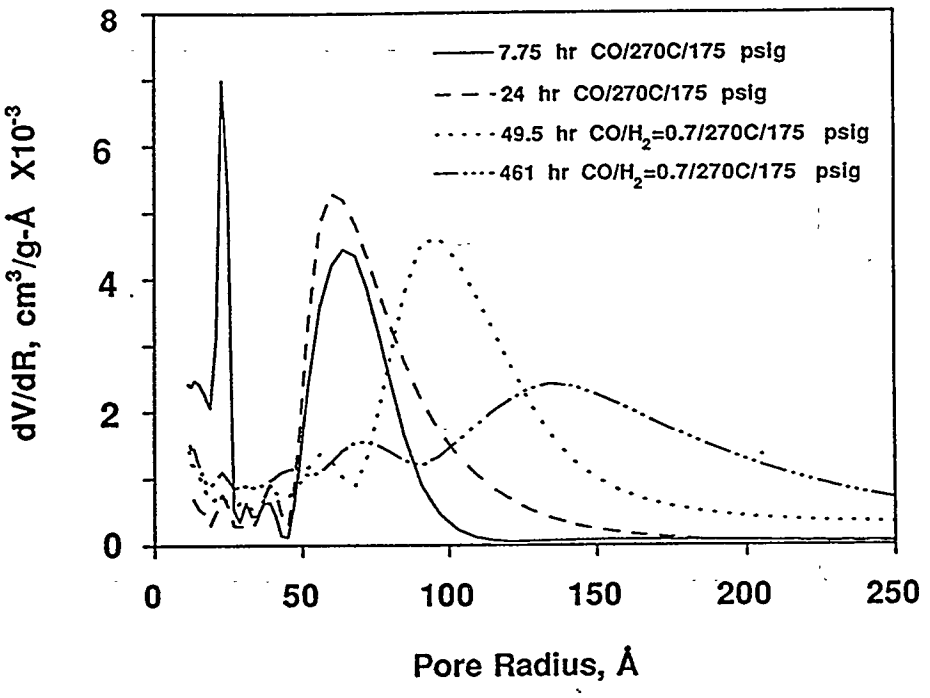

Figure VI.7.35. Pore size distribution of RJO-137 following 7.75 hr and 24 hr at pretreatment conditions and 49.5 hr and 461 hr at synthesis conditions.

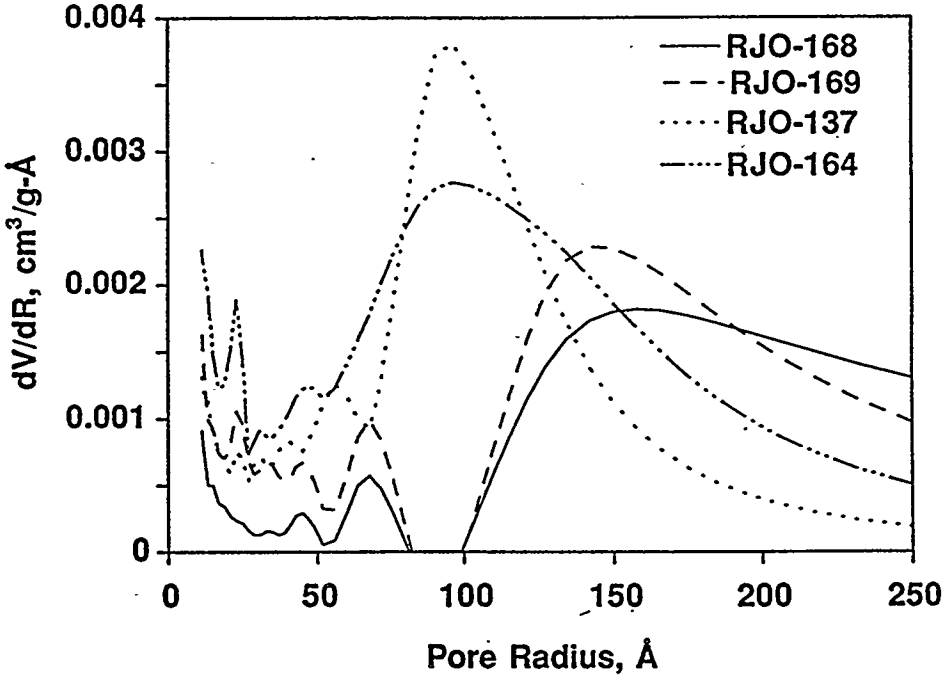

Figure VI.7.36. Pore size distribution of RJO-168, RJO-137, and RJO-164 after 72 hr at synthesis conditions and RJO-169 after 146 hr of synthesis.

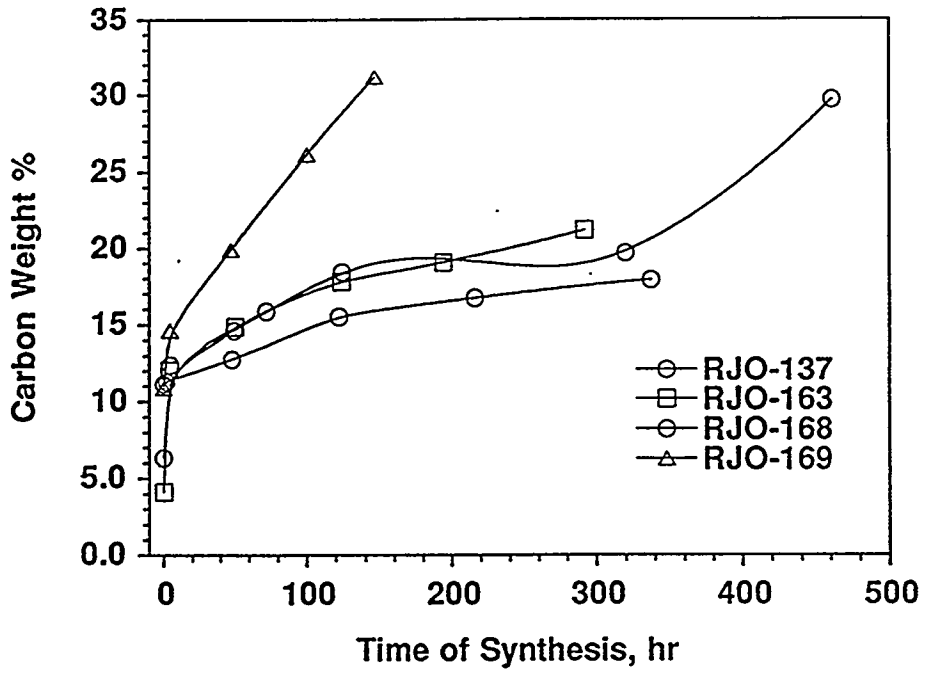

Figure VI.7.37. Weight % of free carbon in catalyst as a function of time of synthesis for RJO-137, RJO-163, RJO-168 and RJO-169.

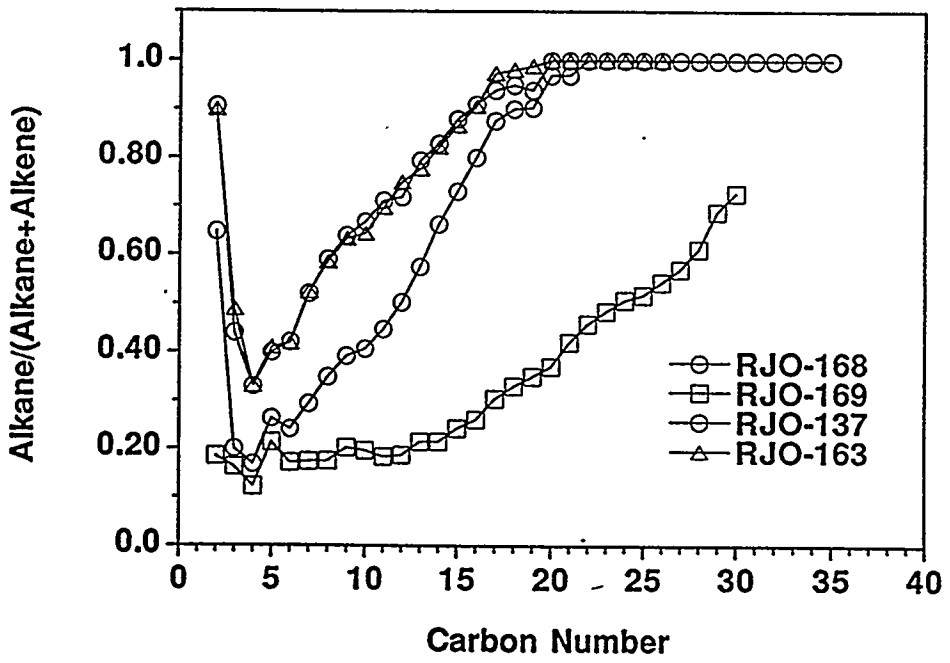

Figure VI.7.38. Alkane/alkene selectivity as a function of carbon number for RJO-168, RJO-169, RJO-137 and RJO-163 after 216, 145, 383 and 290 hr of synthesis, respectively.

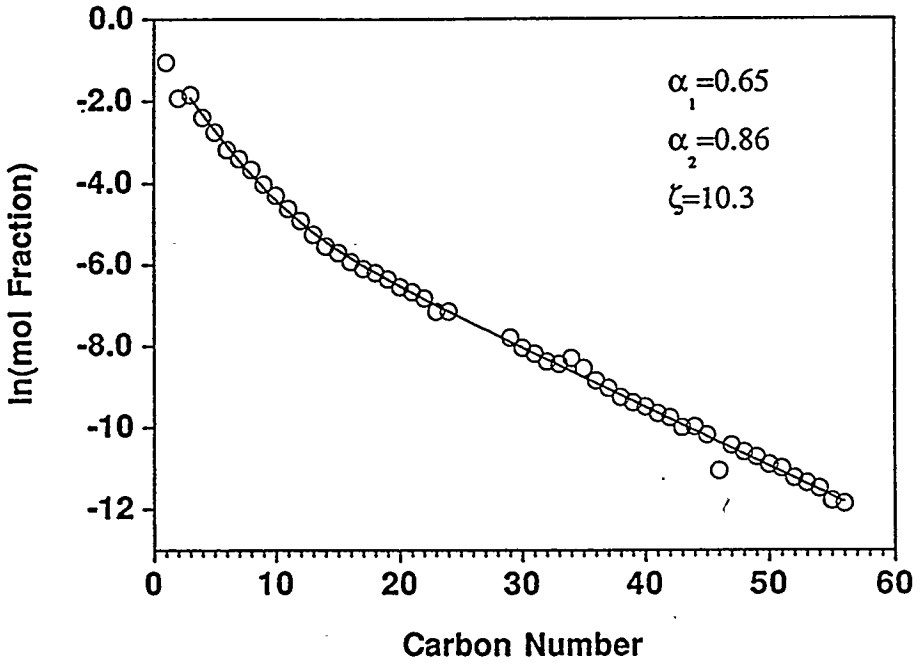

Figure VI.7.39. Anderson-Shulz Flory plot of RJO-163 after 290 hr of synthesis.